Structures of the Siroheme- and Fe_4S_4-Containing Active Center of Sulfite Reductase in Different States of Oxidation: Heme Activation via Reduction-Gated Exogenous Ligand Exchange[†,‡]

Brian R. Crane,[§] Lewis M. Siegel,[||] and Elizabeth D. Getzoff*[,§]

Department of Molecular Biology and The Skaggs Institute for Chemical Biology, The Scripps Research Institute, La Jolla, California 92037, and Department of Biochemistry, Duke University Medical Center, Durham, North Carolina 27710

Received May 7, 1997; Revised Manuscript Received July 25, 1997[⊗]

ABSTRACT: The active center of the *Escherichia coli* sulfite reductase hemoprotein (SiRHP) is exquisitely designed to catalyze the six-electron reductions of sulfite to sulfide and nitrite to ammonia. Refined high-resolution crystallographic structures of oxidized, two-electron reduced, and intermediately reduced states of SiRHP, monitored by single-crystal electron paramagnetic resonance (EPR) spectroscopy, reveal that a bridging cysteine thiolate supplied by the protein always covalently links the siroheme (iron isobacteriochlorin) to the Fe_4S_4 cluster, facilitating their ability to transfer electrons to substrate. The reduction potential and reactivity of the cluster are tuned by association with the siroheme, accessibility to solvent, and hydrogen bonds supplied by the protein loops containing the four cluster-ligating cysteines. The distorted conformation of the siroheme recognized by the protein potentially destabilizes the electronic conjugation of the isobacteriochlorin ring and produces axial configurations for some propionate side chains that promote interactions with exogenous ligands and active-site residues. An extensive hydrogen-bond network of positively charged side chains, ordered water molecules, and siroheme carboxylates coordinates, polarizes, and influences the protonation state of anionic ligands. In the oxidized (siroheme Fe^{3+}, $Fe_4S_4^{2+}$) SiRHP crystal structure, the high density of positive charges in the binding pocket is stabilized by the siroheme's sixth axial ligand—an exogenous phosphate anion. Binding assays with $H^{32}PO_4^{2-}$ demonstrate that oxidized SiRHP binds phosphate in solution with a dissociation constant of 14 μM at pH 7.7, suggesting that phosphate anions play an important role in stabilizing and sequestering the active-site of the oxidized enzyme *in vivo*. Reduction of the cofactors couples changes in siroheme iron coordination geometry to changes in active-site protein conformation, leading to phosphate release both in the crystal and in solution. An intermediately reduced enzyme, where the siroheme is mainly ferrous (+2) and the cluster cubane is mainly oxidized (+2), appears to have the lowest affinity for phosphate in the crystal. Reduction-gated release of phosphate from the substrate-binding site may explain the 10^5-fold increase in rates of ligand association that accompany reduction of SiRHP.

Sulfite reductases (SiRs)[1] and related nitrite reductases (NiRs) are the only known class of enzymes that couple a metalloporphyrin to an iron−sulfur cluster in the construction of a catalytically active redox center. In this center, the siroheme (an iron−tetrahydroporphyrin of the isobacteriochlorin class) and the Fe_4S_4 cluster, which are bridged by a cysteine thiolate, function cooperatively with the protein to carry out the six-electron reductions of sulfite to sulfide and nitrite to ammonia during the biological assimilation and dissimilation of sulfur and nitrogen compounds (Siegel *et al.*, 1973; Peck & Lissolo, 1988). The *Escherichia coli* assimilatory sulfite reductase, a component of the cysteine regulon that functions to reduce sulfite to sulfide for incorporation into cysteine, is constructed from four catalytic hemoprotein (SiRHP) subunits and eight electron-supplying flavoprotein subunits.

In the 1.6 Å resolution crystallographic structure of oxidized SiRHP (Crane *et al.*, 1995), the siroheme and Fe_4S_4 cluster are bound at the interface of three α/β-type domains (domain 1/1′ or the "parachute" domain, domain 2, and domain 3; see Figure 1A). An apparent gene duplication has constructed the protein from two pseudosymmetric halves, termed sulfite or nitrite reductase repeats (SNiRRs). The N-terminal SNiRR, composed of subdomain 1 (secondary structural elements $\beta1-\beta4$ and $\alpha1-\alpha2$) and domain 2 ($\beta5-\beta9$ and $\alpha3-\alpha5_b$) and a C-terminal SNiRR composed

† This work was supported by NIH Grants GM37684 to E.D.G. and GM212226 to L.M.S. and by an NSERC 1967 fellowship to B.R.C.

‡ PDB codes for the structures reported herein: HP−PO_4, 1AOP; HP−PO_4 CrII, 2AOP; HP−PO_4 PR1, 3AOP; HP−PO_4 PR2, 4AOP; HP_{Em} CrII, 5AOP.

* Author to whom correspondence should be addressed.

§ The Scripps Research Institute.

|| Duke University Medical Center.

⊗ Abstract published in *Advance ACS Abstracts,* September 15, 1997.

[1] Abbreviations: CHES, 2-(*N*-cyclohexylamino)ethanesulfonic acid; DE52, (diethylaminoethyl)cellulose, type 52; HEPES, *N*-(2-hydroxyethyl)piperazine-*N*′-2-ethanesulfonic acid; EDTA, ethylenediaminetetraacetic acid; ENDOR, electron nuclear double resonance; EPR, electron paramagnetic resonance; HOMO, highest occupied molecular orbital; HP, oxidized sulfite reductase hemoprotein (siroheme Fe^{3+}, $Fe_4S_4^{2+}$); HP −1, one-electron reduced sulfite reductase hemoprotein (siroheme Fe^{2+}, $Fe_4S_4^{2+}$); HP −2, two-electron reduced sulfite reductase hemoprotein (siroheme Fe^{2+}, $Fe_4S_4^{1+}$); KP_i, potassium phosphate buffer, pH 7.7; NADPH, nicotinamide adenine dinucleotide phosphate; NiR, nitrite reductase; MV^+, reduced methyl viologen; PAGE, polyacrylamide gel electrophoresis; PEG, poly(ethylene glycol); SFe, siroheme iron; SiR, sulfite reductase; SiRHP, sulfite reductase hemoprotein; SNiRR, sulfite or nitrite reductase repeat; SSRL, Stanford Synchrotron Radiation Laboratory.

S0006-2960(97)01065-9 CCC: $14.00

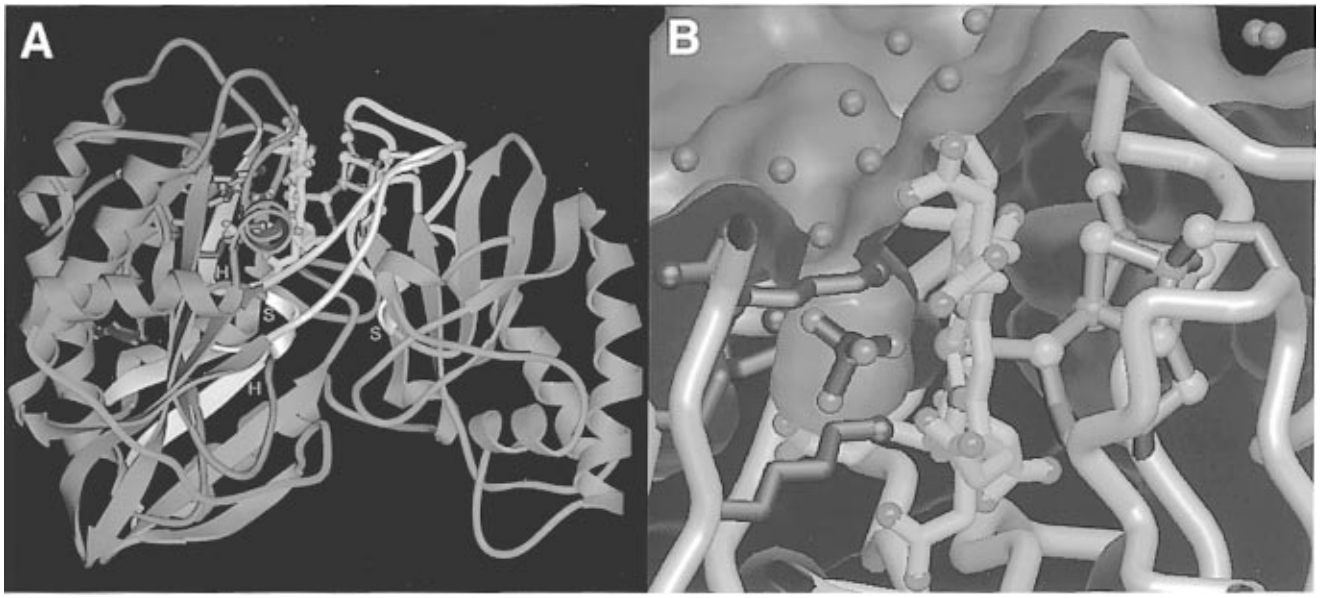

FIGURE 1: (A) Overall topology of SiRHP showing the position of the active center and loops involved in binding the cofactors. The molecule is constructed from an N-terminal SNiRR (cyan) and a C-terminal SNiRR (magenta) that are related by a pseudo-2-fold axis of symmetry and joined by a 17-residue linker strand (green). The siroheme (gold bonds, with red oxygen, blue nitrogen, and brown iron atoms, top center) interacts with residues on loops supplied from the parachute domain, domain 2, and the spiral connection of domain 3 (white regions), whereas the Fe_4S_4 cluster (green bonds with yellow sulfur and brown iron atoms, right) is coordinated by two loops (yellow) supplied by domain 3. Phosphate (purple with red oxygens) coordinates the siroheme and binds in a pocket containing positively charged Lys and Arg residues (blue, top left) supplied from β-strands in the N-terminal SNiRR. β3 (β3′), β4 (β4′), and their interposed harness turns (behind, white, and labeled cyan H for the N-terminal SNiRR and magenta H for the C-terminal SNiRR) along with the spiral connections (center, white, and labeled S) integrate the cofactors at the interface of SiRHP's three domains. (B) Closeup of the oxidized SiRHP active center shown with a solvent-accessible surface (same orientation as in panel A). The siroheme (center, same colors as in panel A) and Fe_4S_4 cluster (right) are closely associated with the SiRHP protein (white tubes). The protein provides a cysteine thiolate to covalently bond the siroheme iron (brown) to the closest Fe_4S_4 iron cluster's iron (brown). Two adjacent loops (right) project from the domain 3 β-sheet to supply four cysteine thiolates to coordinate the Fe_4S_4 cluster and protect the cubane from solvent. Phosphate (purple), an axial siroheme ligand, is bound in a pocket formed by the siroheme and four positively charged residues (blue) that extend from β strands of domains 1′ and 2 (left). Ordered water molecules (blue spheres) line the solvent-accessible surface of the active-site cleft [purple, calculated with MS (Connolly, 1983), 1.4 Å probe radius], and one interacts with the only accessible phosphate oxygen atom.

of domain 1′ (β1′−β4′ and α1′−α2′) and domain 3 (β5′−β9′ and α3′−α5′) are associated by a pseudo 2-fold rotation axis that generates a single, internally symmetric parachute domain from subdomains 1 and 1′ and relates domain 2 to domain 3 (see Figure 1A). Two symmetrically related "harness turns" of the parachute, formed between β3 and β4 of domain 1 and β3′ and β4′ of domain 1′ along with two 3_{10} "spiral connections" between β6 and β7 of domain 2 and β6′ and β7′ of domain 3, participate in binding the cofactors at the interdomain interface (Crane *et al.*, 1995). The two SNiRRs are joined by a 17 residue extended "linker strand" that structurally mimics the ligand-bound siroheme in a cavity symmetry-related to the active center (Crane *et al.*, 1995). In the oxidized enzyme as isolated, a highly adapted anion-binding cavity, formed on the distal side of the siroheme by subdomain 1 and domain 2, contains a phosphate molecule bound axially to the siroheme (see Figure 1B). Hydrogen-bond networks integrate the bound phosphate with ordered water molecules, the siroheme carboxylates, and positively charged protein side chains extending from the surrounding β strands. Domain 3 positions the Fe_4S_4 cluster proximal to the ruffled siroheme and supplies the bridging Cys483 thiolate that coordinates both the cluster and the siroheme iron.

EPR (Janick & Siegel, 1982), Mössbauer (Christner *et al.*, 1983), ENDOR (Cline *et al.*, 1985), resonance Raman (Madden *et al.*, 1989) and paramagnetic NMR (Kaufman *et al.*, 1993) spectroscopies indicate that the siroheme and iron−sulfur cluster are closely associated and electronically influenced by one another in all oxidation states of the enzyme. Three stable oxidation states participate in SiRHP's catalytic cycle (Siegel *et al.*, 1982; Janick & Siegel, 1982; Janick *et al.*, 1983): (1) an oxidized state (HP) with a ferric (Fe^{3+}) siroheme iron (SFe) and an Fe_4S_4 cubane with a formal charge of +2 ($Fe_4S_4^{2+}$), (2) a one-electron reduced state (HP −1) with a ferrous (Fe^{2+}) siroheme iron and an $Fe_4S_4^{2+}$ cluster, and (3) a two-electron reduced state (HP −2) with a ferrous (Fe^{2+}) siroheme iron and an $Fe_4S_4^{1+}$ cluster. The similarity of the reduction potentials for the siroheme [−340 mV (Siegel *et al.*, 1982)] and the cluster [−405 mV (Janick & Siegel, 1982)] imply a distribution of the above states in an intermediately reduced enzyme at equilibrium. *In vivo*, the hemoprotein subunits receive electrons from associated flavoprotein subunits, which are themselves reduced by NADPH, while *in vitro*, the isolated hemoprotein subunits are catalytic when reduced by suitable nonnatural electron donors such as reduced methyl viologen (MV^+) or Cr(II) EDTA (Siegel & Davis, 1974; Janick & Siegel, 1982, Madden *et al.*, 1989).

In the oxidized state, the ferric siroheme is high-spin ($S = {}^5/_2$) and the $Fe_4S_4^{2+}$ cluster is diamagnetic. In the one-electron reduced state, Mössbauer studies indicate that the ferrous siroheme is of integral spin, either high ($S = 2$) or intermediate ($S = 1$) (Christner *et al.*, 1983), while resonance Raman studies conclude that the siroheme is of either low ($S = 0$) or intermediate spin ($S = 1$) (Han *et al.*, 1983*b*). An intermediate spin state for the one-electron reduced enzyme, also supported by paramagnetic NMR studies (Kaufman *et*

al., 1993), is unusual because porphyrins in this spin configuration generally do not possess axial ligands (Scheidt & Reed, *et al.*, 1981). In solution, the $S = {}^1/_2$ $Fe_4S_4^{1+}$ cluster of the two-electron reduced enzyme is predominantly coupled to a high-spin ($S = 2$) ferrous siroheme (Han *et al.*, 1989b), whereas in the frozen state the $S = {}^1/_2$ cluster is coupled to a mixture of of high- ($S = 2$), intermediate- ($S = 1$), and low-spin ($S = 0$) siroheme species (Janick & Siegel, 1982; Christner *et al.*, 1983).

Compared to the oxidized enzyme, the reduced states of SiRHP react 10^5 times more quickly with substrates and heme ligands (Janick *et al.*, 1983). However, if the oxidized enzyme is reversibly reduced and oxidized in CHES buffer at pH 9.5, its rate of reaction with ligands also increases by 3 orders of magnitude (Young & Siegel, 1988b). This activated state relaxes to an inactivated state with time and on titration back to neutral pH with phosphate buffer. The discovery of a phosphate anion bound in the substrate-binding site of the oxidized enzyme (Crane *et al.*, 1995) suggests that this anion may act as an inhibitor and thereby be responsible for the oxidized enzyme's slow rates of association with ligands. Herein we describe in depth the active-center architecture and cofactor assembly of SiRHP under various reducing conditions and report a potentially physiologically relevant mechanism of SiRHP activation that involves release of phosphate from the active center on reduction of the enzyme's prosthetic groups.

EXPERIMENTAL PROCEDURES

Except where stated, all chemicals were purchased from Sigma Chemical Co.

Protein Expression and Purification. SiRHP was expressed and purified from the pBR322 plasmid derivative pJYW613, kindly provided by Drs. J. Wu and N. M. Kredich (Duke University Medical Center, Durham, NC). pJYW613 contains *E. coli B cysI*, which codes for SiRHP, *E. coli B cysJ*, which codes for SiRFP, and *Salmonella typhimurium cysG*, which codes for a methyltransferase necessary for the conversion of uroporphyrinogen III to siroheme (Wu *et al.*, 1991). All three genes are under control of the *cysJIH* promoter and thus require limiting reduced sulfur for overexpression. For expression of *E. coli* SiR holoenzyme, pJYW613 was transformed by electroporation into *S. typhimurium* strain cysI68, which does not produce endogenous SiRHP. *S. typhimurium* strain LB5000 that is r^- m^+ for all three *S. typhimurium* restriction modification systems was used to suitably restrict *E. coli* pJYW613 for introduction into the cysI68 strain. The transformed cysI68 strain was grown in modified LeMaster medium (Hendrickson *et al.*, 1990), which contained sulfate as the sole sulfur source. SiRHP was purified as reported (Siegel *et al.*, 1973; Kaufman *et al.*, 1993) with the following minor modifications: (1) For the removal of nucleic acids by protamine sulfate treatment, 5% protamine sulfate was slowly added to the cell lysate in the presence of 1 M KCl to prevent the SiR holoenzyme from binding to the protamine sulfate. (2) After the second ammonium sulfate cut, the resuspended pellet containing the 800 kD holoenzyme was chromatographed over a Pharmacia Superose-12 gel-filtration column equilibrated with 50 mM potassium phosphate (KP_i) and 100 μM EDTA. The holoenzyme was then dialyzed overnight into 4 M urea and 10 mM potassium phosphate, pH 7.7, to dissociate the hemoprotein from the flavoprotein subunits. The hemoprotein subunits were resolved from the flavoprotein subunits by eluting the dissociated holoenzyme from a Whatman DE52 cellulose column with 50 mM potassium phosphate in 4 M urea [see also Siegel and Davis (1974)].

Crystal Growth and Mounting. Prior to crystallization, SiRHP at 10 mg/mL in 65 mM potassium phosphate (pH 7.7) and 100 μM EDTA was treated with 5 μg/mL trypsin for 17 h at room temperature to remove the N-terminal 73 residues (Crane *et al.*, 1995). For the reduction and complexation studies, all crystals were grown anaerobically in a Coy Industries anaerobic glove bag under an atmosphere of 97% N_2 and 3% H_2. All solutions were purged with Ar on a Schlenk line before introduction into the glove bag. SiRHP crystals of space group $P2_12_12_1$ and unit cell dimensions 69.8 × 77.4 × 87.8 Å^3 (McRee *et al.*, 1986) were grown in sitting drops containing 4−5 mg/mL SiRHP in 65 mM KP_i, pH 7.7, and 9% poly(ethylene glycol) (PEG) MW 8000 (KP_i/PEG) by vapor diffusion against 65 mM KP_i, pH 7.7, and 15−20% PEG 8K. The purified PEG (Hampton Research) used in crystallizations contained low levels of oxidizing agents (peroxides < 0.00003% and aldehydes < 0.0005%) and did not noticeably reoxidize millimolar concentrations of reduced methyl viologen (MV^+, blue in color when reduced and clear when oxidized) over a period of days. Large single crystals (typically 0.15 × 0.2 × 0.8 mm^3) were produced by successive macroseeding into sitting drops containing decreasing concentrations of PEG MW 8000 from 15% to 11%. Crystals were mounted anaerobically in glass or quartz capillaries, flame-sealed at one end prior to introduction into the anaerobic hood. A plug of mother liquid containing MV^+ was placed near the open end of the capillary to monitor any reoxidation by air after sealing. Capillaries sealed in the glove bag, first with quick-drying epoxy and then with nail polish, remained anaerobic for weeks when exposed to aerobic conditions. All crystals to be exposed to synchrotron radiation were mounted in sealed capillaries in our anaerobic hood at Scripps, as described above, and then transported to the Stanford Synchrotron Research Lab (SSRL) in two layers of glass jars with screw tops sealed under nitrogen.

Reduction of SiRHP Crystals with Cr(II) EDTA. The powerful reductant Cr(II) EDTA (midpoint potential $E^{\circ\prime} \simeq -1.0$ V) is highly effective at reducing SiRHP in solution (Madden, 1990). Cr(II) EDTA was prepared in the anaerobic glove bag as follows and as described in Han *et al.* (1989b). $Cr(II)Cl_2$ (0.5 M) (Aldrich) was dissolved in 0.5 M HCl and then 300 μL of this solution was added to 700 μL of 0.5 M EDTA, pH 5.1, to produce stock 150 mM Cr(II) EDTA. This solution would change from a pale blue to a light purple color (indicative of oxidation) over the period of a few hours, but would then maintain its color and the ability to reduce methyl viologen [$E^{\circ\prime} = -446$ mV (Kuwana, *et al.*, 1977)] for days.[2] Exposure to air resulted in an immediate color change to dark purple and loss of all reducing activity. Stock Cr(II) EDTA was diluted into KP_i/PEG or 130 mM HEPES, 15% PEG 8K, pH 7.7 (HEPES/PEG), to give concentrations of 1−20 mM. At 10 mM, the concentration of Cr(II) EDTA used for the preparation of most complexes, the pH of KP_i/PEG drops from 7.7 to 7.3 due to the acidity of the Cr(II)

[2] Cr(II) EDTA is known to undergo slow spontaneous oxidation in aqueous solution which is likely caused by the reduction of water or soluble ions (Thompson & Sykes, 1976).

Table 1: Diffraction Data and Refinement Statistics for the Crystallographic Structures of SiRHP in Various Oxidation States

structure[a]	ligand[b]	oxid. state[c]	res'n[d] (Å)	R_{sym}[e] (%)	$I/\sigma I$ [f]	comp[g] (%)	R-factor[h] (%)	comp[i] (%)	rmsd geom[j]	waters[k]	$\langle B\rangle$[l] (Å^2)	$\langle \Delta r\rangle$[m] (Å)	PDB code
HP−PO_4[n]	HPO_4^{2-}	0	1.60	9.9	28.7	96.7	18.2	96.7	0.010	486	19.8	0.14	1aop
			1.76−1.60	27.0	7.5	93.5	27.8	93.5	1.6				
HP−PO_4 CrII[o]	HPO_4^{2-}	−2	1.75	6.6	18.6	97.8	17.5	97.8	0.009	424	22.4	0.15	2aop
			1.81−1.75	33.6	3.6	95.4	25.1	93.9	1.5				
HP−PO_4 PR1[o]	HPO_4^{2-}	−2	2.10	9.2	16.6	99.5	16.7	97.2	0.010	383	24.7	0.27	3aop
			2.00−2.10	26.9	5.4	99.9	20.5	96.7	1.6				
HP−PO_4 PR2[o]	HPO_4^{2-} + H_2O	m	1.80	7.0	19.0	96.4	17.5	92.3	0.010	384	28.6	0.17	4aop
			1.86−1.80	28.9	4.9	95.2	25.3	82.4	1.6				
HP_{Em} CrII[o]		−2	2.20	9.6	12.2	99.4	16.4	96.3	0.009	352	23.4	0.20	5aop
			2.28−2.20	30.3	3.7	99.7	20.5	92.3	1.5				

[a] CrII stands for reduction by Cr(II) EDTA, while PR stands for photoreduction by a flavin/EDTA-coupled system (1 and 2 being different crystals reduced under different conditions). [b] Bound ligand(s). In HP_{Em} CrII, the distal anion-binding site is empty. [c] Presumed predominant oxidation state relative to oxidized SiRHP (Fe^{3+} siroheme, $Fe_4S_4^{2+}$ cluster). A mixed oxidation state containing contributions from HP, HP −1, and HP −2 is referred to as m. [d] Maximum resolution of the diffraction data (upper entry) and range of resolution in the highest bin for compiling statistics (lower entry). [e] $R_{sym} = \sum_j|I_j - \langle I\rangle|/\sum_j I_j$, over all data (upper entry) and in highest resolution range (lower entry). [f] Intensity signal to noise ratio. [g] Completeness of unique diffraction data. [h] R-factor $= \sum||F_{obs}| - |F_{calc}||/\sum|F_{obs}|$. [i] Completeness of unique diffraction data used in refinement after σ_{cut} was applied. No σ cutoff on $|F|$ was used for refinement of the oxidized structure, although only $|F| \geq 2\sigma|F|$ was used in refinement of the other species. [j] Root mean square deviation of model bond lengths (upper entry, in angstroms) and angles (lower entry, in degrees) from ideal geometry. [k] Number of water molecules included in the refinement. [l] Average model thermal (B) factor. [m] Average coordinate error estimated from a σ_A plot (Read, 1988). [n] Diffraction data were collected on a 30 cm Mar Research image plate detector at the Stanford Synchrotron Radiation Laboratory (SSRL), beam line 7-1 (1.08 Å radiation) and processed with MOSFLM (Leslie *et al.*, 1986). [o] Mar Research 30 cm image plate detector, SSRL beam line 7-1, processed with DENZO (Otwinowski *et al.*, 1993). All diffraction data were collected at 4 °C.

EDTA reagent. (SiRHP crystals are tolerant of pHs from 5.5 to 8.5.) Crystals were soaked for various durations in sealed wells with 100 μL of these reducing solutions. A reduced SiRHP species without any ligand bound in the active site (HP_{Em} CrII) was prepared by soaking a crystal for 20 min in 10 mM Cr(II) EDTA/HEPES/PEG.

Photoreduction of SiRHP Crystals. Crystals were mounted in glass or quartz capillaries and surrounded by 8 μL of photoreducing solution (typically 65 mM KP_i, pH 7.7, 15% PEG 8K, 10 or 50 mM EDTA, and 750 μM proflavin). Photoreduction was carried out by irradiating the sample for various durations with a Nikon MKII fiber-optic light source containing a 21 V−150 W halogen bulb. Photoreductant was then removed and the crystals were either dried with a paper wick, back-soaked with KP_i/PEG, or left in a small plug of mother liquor before the capillary was sealed.

Diffraction Data Collection and Reduction. Diffraction data for the various complexes and reduction states of SiRHP crystals were collected with a variety of synchrotron and conventional X-ray sources summarized in Table 1. The data sets, which ranged in resolution from 1.6 to 2.1 Å, were reduced with software that was appropriate and convenient for the data collection device and locality (see Table 1).

Fourier Analysis, Model Building, and Refinement. Relative scaling of data sets and calculation of $2F_o - F_c$, $F_o - F_c$, and omit Fourier electron density maps were accomplished with the XtalView software package (McRee, 1992). XFIT, contained in XtalView, was used for model building and structural analysis, while all refinement of crystallographic models was carried out with X-PLOR (Brünger *et al.*, 1987). For the structure determination of SiRHP reduced states, a previously refined model of oxidized SiRHP at 1.6 Å resolution (Crane *et al.*, 1995, 1997a; Crane & Getzoff, 1997), with the phosphate and water molecules removed, was refined by positional refinement in X-PLOR against the new diffraction data, first to 2.8 Å and then to 2.2 Å (or to the limit of the data's resolution). The loops and areas surrounding the active center were rebuilt to simulated annealed $F_o - F_c$ omit electron density maps (Hodel *et al.*, 1992), whereas the rest of the molecule, which changed little in conformation, was surveyed and adjusted with standard $F_o - F_c$ and $2F_o - F_c$ maps. Ligands were modeled into the resulting difference peaks on the distal side of the siroheme, resolution was extended, and water molecules were added gradually over cycles of positional conjugate gradient refinement followed by B-factor refinement. Water molecules were placed only in difference peaks greater than 3σ that were 2.2−3.5 Å from appropriate protein hydrogen-bonding partners. The number of water molecules added was dependent on the resolution of the diffraction data (see Table 1). When data quality and resolution permitted, restraints were completely removed from the iron−sulfur cluster, bridging ligand, and siroheme iron in the last stages of refinement. In all crystals treated with reductant, the structural changes were small and localized to the active center and its surrounding loops. Application of an overall anisotropic thermal factor to the diffraction amplitudes by X-PLOR diminished noise in the difference Fouriers and improved R-factors. Components of the overall anisotropic thermal factor were small but consistent for all of the reported structures and indicated slightly more disorder along b^* ($\langle B_{11}\rangle = -1.9$ Å^2, $\langle B_{22}\rangle = 2.8$ Å^2, $\langle B_{33}\rangle = -0.8$ Å^2). There is no obvious correlation between this anisotropy and the crystal shape or packing.

EPR Spectroscopy. EPR spectra were measured with a Brüker ESP-300 EPR spectrometer equipped with an Air Products LTR-3 Helitran cryostat and operating at X-band (9.51 GHz). Samples were measured at 9 K, with a modulation frequency of 100.0 kHz, a modulation amplitude of 20 G, a power of 2.00 mW, and a receiver gain of 8×10^5. Although the amount of protein in a single SiRHP crystal is small compared to standard EPR solution samples, the signals are still measurable, because the magnetic moments involved are not isotropically averaged as they are in solution. However, as a result, single-crystal EPR spectra are complicated by the orientation dependence of the signal intensity and field value. The space group symmetry of $P2_12_12_1$ for SiRHP generates four unique molecular orienta-

tions in each crystal. For one molecular orientation, the normal to the plane formed by the pyrrole and pyrroline nitrogens of the siroheme in the oxidized SiRHP structure is 39° from the crystallographic ***a*** axis, 76° from the ***b*** axis, and 55° from the ***c*** axis. The three other molecular orientations are generated by 222 crystallographic symmetry. Reduction of the siroheme should result in loss of the low field $S = {}^5/_2$ high-spin signal observed for crystals of the oxidized enzyme. Although EPR signals from the reduced Fe_4S_4 cluster (Janick & Siegel, 1995) are too small to be detected from single crystals, we assume reduction of the siroheme by excess Cr(II) EDTA also results in reduction of the Fe_4S_4 cluster because the two prosthetic groups are covalently coupled and the redox potential of the Cr(II) EDTA reagent (<-1.0 V) is far below that of either the siroheme [−340 mV (Siegel *et al.*, 1982)] or the cluster [−405 mV (Janick & Siegel, 1982)]. A decreased high-spin signal would be expected for an intermediately reduced crystal; however, such spectra will not distinguish if a distribution of states centered on the one-electron reduced enzyme is homogenous throughout the crystal or if some molecules are completely reduced while the others are completely oxidized.

For the EPR experiments, the crystals were mounted anaerobically in 1.0 mm diameter, open-ended quartz capillaries, which were then placed in quartz EPR tubes. The EPR tubes were flash-cooled with liquid N_2 in the anaerobic glove bag prior to placement in the liquid helium cryostat. Samples cooled to liquid nitrogen temperatures showed no spectral evidence of reoxidation with time. Crystals were reoxidized by thawing and blowing air down into the EPR tube for varied durations. Because of the orientation dependence of the EPR signals, comparisons of signal intensity between spectra were made only when respective orientations produced signals at the same field values. Although efforts were made to maintain the same crystal orientation before and after oxidation, this process sometimes resulted in rotation of the capillary inside the EPR tube along an axis parallel to the EPR tube. This could be compensated by a rotation of the tube itself in the cryostat. For the reoxidation experiments, EPR spectra were taken on crystals that were successively cooled to 9 K (by first flash-cooling in liquid N_2 to $\sim$ 100 K) and then warmed to room temperature, air-oxidized, and recooled again. The process of thawing and recooling affected the integrity of the crystals and diminished signals on control oxidized crystals by as much as 30%.

Gel Electrophoretic Assays of $H^{32}PO_4^{2-}$ Binding to SiRHP. To demonstrate binding of phosphate to SiRHP in solution, 1.5 μM SiRHP was incubated with 8−200 μM $K_2H^{32}PO_4$ (specific activity 1 mCi/μ mol) in 100 mM HEPES buffer, pH 7.7, at 25 °C in the presence and absence of the substrate sulfite and the reducing agent MV^+, before labeled protein bands were resolved by nondenaturing PAGE and detected by autoradiography. Prior to the experiment, SiRHP was dialyzed extensively against phosphate-free 100 mM HEPES, pH 7.7. MV^+ was quantitated spectrophotometrically using $\epsilon = 13\ mM^{-1}\ cm^{-1}$ at 600 nm and prepared anaerobically by reacting 40 mM methyl viologen dichloride with the Cr(II) EDTA reagent described above. For assays of reduced samples, protein solutions were purged of oxygen and placed under an argon atmosphere in rubber-septum stoppered glass vials prior to the introduction of $H^{32}PO_4^{2-}$ and MV^+ through the septum with an air-tight syringe. Aliquots were extracted, mixed with 3 μL of loading buffer (10 mM Tris, pH 7.7, 75% glycerol, and 0.05% bromophenol blue) and loaded immediately on a 4−20% gradient polyacrylamide gel. Electrophoresis of oxidized and reduced samples was performed over 1 h in 40 mM Tris and 400 mM glycine buffer, pH 7.7 (Tris/glycine), which was extensively degassed prior to the experiment. Following electrophoresis, the gels were washed for 30 min in Tris/glycine running buffer, dried, and exposed to X-ray film at −70 °C.

K_D Measurement for $H^{32}PO_4^{2-}$ Binding to SiRHP. The dissociation constant (K_D) for SiRHP and phosphate was determined using a rapid filtration procedure involving centrifugation of solutions containing phosphate and enzyme through a Microcon 30 microconcentrator (Amicon) to separate free $H^{32}PO_4^{2-}$ from $H^{32}PO_4^{2-}$ bound to SiRHP. Electrophoresis of $H^{32}PO_4^{2-}$-bound SiRHP indicated that phosphate binds to SiRHP over a period of minutes to hours, and thus equilibrium should not be substantially perturbed during the 2 min of centrifugation needed to separate solutions of free ligand. Competition binding assays (Wiener & Reith, 1992) of cold HPO_4^{2-} with $H^{32}PO_4^{2-}$ at two concentrations of the radiolabeled ligand were used to simultaneously determine the specific activity of $H^{32}PO_4^{2-}$ and its K_D with SiRHP.

Over a period of 24 h, 10 μM SiRHP was incubated with 0.1−200 μM cold HPO_4^{2-} in 100 mM HEPES, pH 7.7, in the presence of either 2 or 20 μM $H^{32}PO_4^{2-}$ (total volume of 50 μL). To correct for nonspecific binding of phosphate to the Microcon membranes, blank assays were performed without enzyme in parallel with every binding assay. Before separation of the free fraction by centrifugation, 10 μL was removed from each assay mixture and added to 3 mL of scintillation fluid to provide a measurement of the total radioactive ligand concentration. The remaining solution was then placed in a Microcon-30 (MW cutoff 30 000) microconcentrator and spun for 2 min at 11000g. Ten microliters μL of filtrate, representing the free ligand concentration, was collected and added to 3 mL of scintillation fluid for counting on the ^{32}P channel Beckman scintillation counter. For each titration, the total concentration of labeled ligand was constant and hence all measurements were averaged in the analysis. The presence of the protein attenuated the counts recorded by scintillation and these measurements were appropriately adjusted in comparison to the blank assays. Ligand bound by the protein was determined by subtracting the amount of labeled ligand passing through the filter from the total ligand concentration and then correcting for the nonspecific binding of the filter observed in the blank. Assays were performed in triplicate.

For the competition titrations, assuming that radioactive and nonradioactive ligands have the same affinity for SiRHP

$$\frac{P^*_B}{P^*_B{}^T} = \frac{1}{\dfrac{1+P}{(P^* + K_D)}} \qquad (1)$$

where $P^*_B{}^T$ is the total concentration of $H^{32}PO_4^{2-}$ bound with no cold HPO_4^{2-} present, P^*_B is the concentration of $H^{32}PO_4^{2-}$ bound in the presence of competing HPO_4^{2-}, P is the concentration of cold HPO_4^{2-}, P^* is the concentration of active $H^{32}PO_4^{2-}$, and K_D is the dissociation constant for

phosphate and SiRHP. ($P^* + K_D$) represents the concentration of cold phosphate that will displace half of the bound radiolabeled phosphate at the fixed concentration of P^* (C_{50}). Thus, a plot of ${P^*}_B^T/{P^*}_B$ vs P will have a slope of $1/C_{50}$. If the experiment is performed at two concentrations of P^* that are related by a set dilution, two C_{50} measurements will determine P^* and K_D simultaneously, i.e.

$$C_{50}{}^1 = P^* + K_D \quad (2)$$

$$C_{50}{}^2 = 10P^* + K_D \quad (3)$$

In this analysis, the dissociation constant determined will be independent of a constant concentration of an unlabeled competitive inhibitor; therefore radioactive decay of $H^{32}PO_4^{2-}$ to $SO_4{}^{2-}$, a potential phosphate analogue, will not affect measurement of the K_D.

RESULTS AND DISCUSSION

In this section we first describe in detail the structure of oxidized SiRHP's active center in complex with phosphate (Figure 1), with emphasis placed on the structural features important for mediating cofactor reactivity and enabling catalysis. We then confirm that in solution phosphate binds to SiRHP with high affinity and demonstrate that reduction of the cofactors releases this anion to allow substrate binding. Finally, we report five structures of SiRHP in various states of reduction (Table 1). The structural perturbations observed upon reduction are limited to the active center, located at the hub of the enzyme's three domains (Figure 1A), and influence the coordination state of the siroheme and the enzyme's interaction with phosphate.

The Active Center in Oxidized SiRHP (HP−PO4). The high resolution (1.6 Å), quality ($R_{sym} = 9.9\%$, $I/\sigma I = 28.7$), completeness (96.7%), and redundancy (6.2) of the diffraction data (Table 1) for the oxidized phosphate-bound form of SiRHP (HP−PO_4) allowed the crystallographic refinement to be completed without stereochemical restraints on the Fe_4S_4 cluster, the bridging ligand, siroheme iron, and the siroheme torsion angles. Thus, the conformation and geometry of the cofactor assembly was determined primarily by the diffraction data alone.

(A) Covalently Coupled Cofactors. The cysteine thiolate shared by the siroheme and Fe_4S_4 cluster couples the prosthetic groups together both structurally and electronically (Figures 1 and 2). The 2.84 Å bond between the ferric, high spin ($S = {}^5/_2$) siroheme iron and the cysteine Sγ of Cys483 is unusually long when compared to other protein and model compound thiolate-to-heme iron bonds.[3] The closest Fe−Fe separation between the siroheme iron and cluster is 4.48 Å (to cluster Fe4), whereas the closest noncovalent separation between the prosthetic groups is a 3.63 van der Waals contact between the Fe_4S_4 inorganic sulfur (S1) and the meso carbon (CHB) separating the pyrroline rings (Figure 2). Torsional angles for bridging Cys483 (Table 2) are atypical for cysteine thiolate metal ligands, which prefer gauche$^-$ (60°) or trans (180°) $\chi 1$ angles and correlated Fe−Sγ−Cβ−Cα torsion angles of 90°, 180°, or 270° (Chakrabarti, 1989). The usual stereochemistry appears to reflect the staggered alignment of the Fe−Sγ and Cβ−Cα bonds between thiolate lone pair orbitals possessing strong orthogonal pπ character. In contrast, the trigonal pyramidal stereochemistry of Cys483 Sγ suggests sp^3 hybridization to a first approximation, with the Sγ−Cβ and lone pair orbital both projected roughly parallel to the siroheme plane and along the CHA−CHC and CHB−CHD methynic axes, respectively (Figure 2). If one assumes a typical heme O_h ligand field, these directions are approximately parallel to the siroheme iron d_{xy} orbital and lie between the downwards projected siroheme iron d_{xz} and d_{yz} orbitals. This places the Cys483 Cβ protons close to the acetate and methyl protons of the siroheme B ring, consistent with results from paramagnetic shifted NMR experiments.[4] The relatively long Cys483 thiolate-to-siroheme iron bond, the additional covalent interaction between the Sγ and the Fe_4S_4 cubane, and the orientation of the lone pair orbital offset from the d_{xz} and d_{yz} orbitals all suggest that the bridging Cys483 thiolate has a relatively weak π-interaction with the high-spin, ferric siroheme iron of oxidized SiRHP.

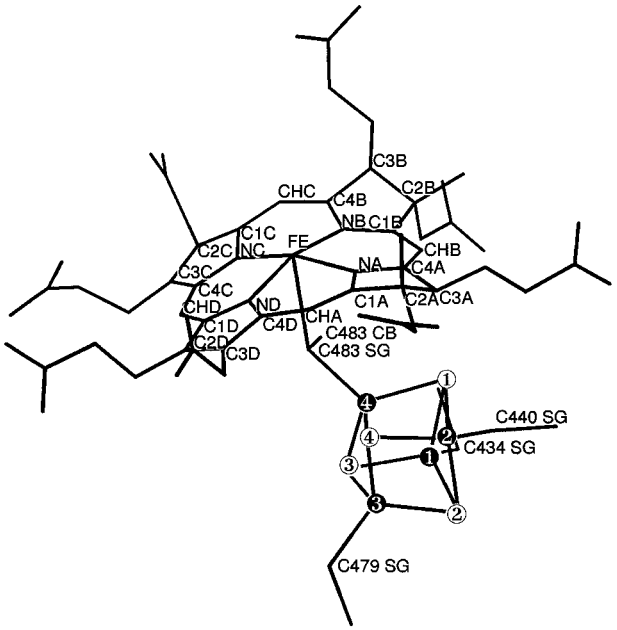

FIGURE 2: Structure and nomenclature of the siroheme−Fe_4S_4 cluster assembly in the active center of oxidized SiRHP. Siroheme (top) has two adjacent unsaturated pyrrole rings (C and D at left), each with one acetate and propionate at the 2 and 3 positions, and two adjacent, partially saturated pyrroline rings (A and B at right), each with an additional methyl group at the acetate-carrying carbon. The Fe_4S_4 cubane (bottom) has four iron atoms (white numbers in black circles) coordinated by Cys sulfur atoms (SG) and four inorganic sulfur atoms (black numbers in white circles).

(B) The Fe4S4 Cluster and Coordinating Loops. The Fe_4S_4 cubane is bound near the surface of the protein by four cysteine thiolates (Figures 1A and 3) that are found in sequences of $CysX_5$ Cys and $CysX_3$ Cys on the first two

[3] Typical thiolate-to-heme iron bonds range from 2.32 to 2.36 Å in length and are relatively insensitive to the oxidation state, spin state, and coordination number of the heme iron (Scheidt & Reed, 1981). However, longer thiolate-to-iron bonds (2.44, 2.55, and 2.96 Å) are found in a sulfur-bridged iron(III) porphyrin−copper(II) system [Fe(III)−S−Cu(II)] (Schauer *et al.*, 1984).

[4] A cysteine residue, identified by deuterium labeling and implicated as the bridging ligand by downfield paramagnetic shifted resonances, exhibits NOEs between its Cβ−H and resonances assigned as siroheme pyrroline Cα and methyl protons (Kaufman *et al.*, 1993). Cys483 is favorably oriented for presenting Cβ−Hs toward the siroheme pyrrolinic acetate Cα and methyl protons on ring B. There is a slightly longer yet also appropriately directed interaction between the Cβ−H from Cys434 and the acetate Cα protons on this same ring.

Table 2: Refined Fe_4S_4 Coordination Parameters for the HP−PO_4 Complex

Bridging Ligand Geometry					
distance (Å)		bond angles (deg)		dihedral angles (deg)	
SFe[a]−Sγ^{483}	2.84	SFe−Sγ^{483}−Fe4	126.1	SFe−Sγ^{483}−Cβ−Cα[b]	255.0
Fe4−Sγ^{483}	2.17	SFe−Sγ^{483}−Cβ	105.9	Fe4−Sγ^{483}−Cβ−Cα	121.1
Fe4−Sγ^{483}−Cβ	102.8	N−Cα−Cβ−Sγ^{483}	313.0		

Fe_4S_4 Geometry					
ligand	Fe	Sγ−Fe (Å)	bond angles Sγ−Fe−μS[c] (deg)	dihedral angles Fe−Sγ−Cβ−Cα (deg)	χ_1 (deg)
Cys^{434}	Fe1	2.25	107.9, 110.1, 122.4	147.5	71.4
Cys^{440}	Fe2	2.22	103.7, 116.3, 123.1	174.6	187.7
Cys^{479}	Fe3	2.26	104.2, 116.6, 122.2	288.4	80.4
Cys^{483}	Fe4	2.17	101.3, 116.4, 121.4	121.1	313.0

[a] SFe represents the siroheme iron. [b] Pyramidalization (χ) of Cys^{483} Sγ = 46.1°, defined by two dihedral angles: $\chi = \omega$(Fe4−Sγ−Cβ−Cα)−ω(SFe−Sγ−Cβ−Cα) + 180° (modulo 360°); for tetrahedral pyramidalization χ = 60°. [c] Three bond angles from each cysteine thiolate, through its liganded iron to each bonded cluster sulfide.

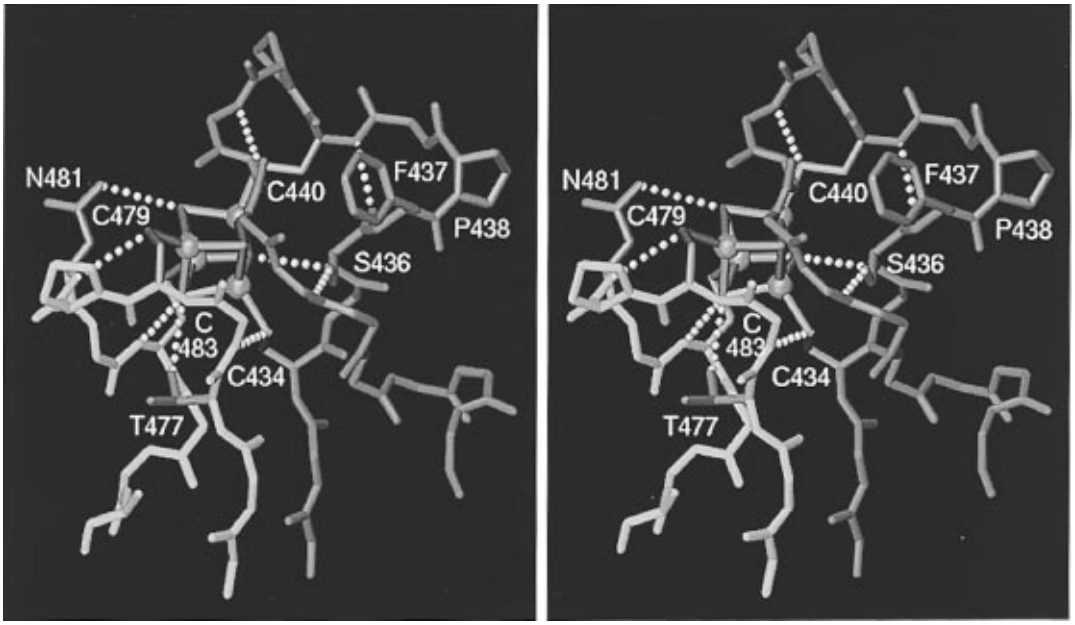

FIGURE 3: SiRHP iron−sulfur cluster structure and environment. Stereo diagram of the SiRHP Fe_4S_4 cubane and main-chain backbone for the first (cyan) and second (yellow) cluster binding loops. The loops shown are depicted as yellow in Figure 1A and the orientation is rotated ~90° about a vertical axis relative to Figure 1A. Parallel hydrogen-bonded β5′ (cyan) and β6′ (yellow) of the C-terminal sheet are shown in the center. The cluster is coordinated by four cysteine thiolates: 434, 440, 479, and 483. The cluster μ-sulfurs and thiolate ligands are hydrogen-bonded (dashed lines) by two peptide nitrogens from the first cluster loop (cyan) and four peptide nitrogens and the Thr477 and Asn481 side chains (magenta) from the second cluster loop (yellow). Uncommon yet compensating geometries for Pro438 and Ser436 (magenta) project Phe437 (magenta) into solvent. The figure was rendered in AVS.

loops succeeding the first two parallel β-strands of the domain 3 β-sheet. The lariat structure of the first cluster loop (Figure 3), C^{434} VSFPTC^{440} X_4 AX_2 E^{448}, buries the cubane from solvent and avoids unfavorable contacts with the siroheme. The lariat is internally anchored by the cluster ligands Cys434 and Cys440, as well as a Ser436 hydroxyl-to-Ala445 carbonyl hydrogen bond across its neck. Direct hydrogen bonds to the siroheme carboxylates and salt bridges to Glu448 from both Arg336 of the linker strand and Arg113 of domain 1 anchor the first cluster loop at the interface of the three SiRHP domains. The 5-residue spacer of the first cluster loop contains structural features that cannot be conserved by the sequences of related SiRs and NiRs (Crane & Getzoff, 1996), suggesting that its conformation may be somewhat variable across the family. In SiRHP, the five residues that space the cysteine ligands cap the cluster and form a structure that resembles a type 2 tight turn (Figure 3). The cis conformation of Pro438 (position $i + 1$, magenta) prevents Phe437 (position i, magenta) from making a tight-turn hydrogen bond with Cys440 (position $i + 3$). Instead, Ser436 (position $i - 1$) assumes a strained backbone conformation to form hydrogen bonds between its peptide carbonyl and the Cys440 peptide nitrogen, its peptide nitrogen and a cluster μ-sulfur (S1), and its hydroxyl and the Ala445 carbonyl. Aromatic residues such as Phe437 are favored to precede cis-peptide bonds (Richardson & Richardson, 1989). The ring of Pro438 participates in a crystal packing contact with Asp295 from a symmetry-related molecule. The unusual yet compensating geometries of Ser436 (ϕ, ψ = 54°, −145°) and cis-Pro438 project intervening Phe437 out into solvent, a seemingly unfavorable orientation possibly relevant for the association and/or electron transfer from the flavoprotein component of SiR rather than for local stability. The sequence variability of these residues in other SiRs and NiRs implies that thiolate bonding with the cubane is a dominant stabilizing factor not dependent on a specific predisposed loop structure. If the spacer size provides sufficient degrees of freedom, alternative

conformations, as seen in the helical $CysX_5Cys$ ligand pattern of the *E. coli* endonuclease III Fe_4S_4 cluster (Kuo *et al.*, 1992), may occur.

The second cluster loop represents the most conserved stretch of sequence throughout the SiR and NiR family (Crane *et al.*, 1995; Crane & Getzoff, 1996), indicating that the tight conformation, hydrogen-bonding pattern to the cluster, and positioning of the bridging ligand, Cys483, place strong constraints on the primary sequence. This second, shorter loop (Figure 3), $G^{478}C^{479}PNG^{482}$ C^{483} G^{484}, wraps tightly around the cubane and then immediately progresses into a type 1-to-3_{10} linked-turn [the "spiral connection" (Crane *et al.*, 1995)] connecting the next parallel strand ($\beta7'$). The only direct hydrogen bond between the two cluster loops is formed between the Gly478 peptide nitrogen and the Cys434 thiolate. Gly482 of the second loop, immediately preceding the bridging ligand Cys483, is in a left-handed conformation, disfavored for other residues. Stringently conserved Gly478 and moderately conserved Gly484 are involved in packing interactions: Gly478 Cα with the carbonyl of Ala445 and Gly484 with the internal sides of $\beta6'$ and $\beta7'$. Interestingly, Gly482, highly substituted in other sequences (Gly, Glu, Ser, Met or Cys), is in a left-handed α conformation (ϕ, ψ = 76°, 25°). The following bridging ligand, Cys483, is at position $i + 1$ of a type 1 turn that is structurally conserved between the two SiRHP SNiRRS and is important for stability of the central interdomain interface. In other SiRs and NiRs, if the second cluster loop is to maintain its conformation and present the bridging ligand, Cys483, for interaction with the siroheme and the Fe_4S_4 cluster, it is necessary for a preceding non-glycine at 482 to be in a potentially strained, left-handed conformation in order to prevent a collision between its Cβ and the cubane.[5]

The +2/+1 redox couple of the SiRHP Fe_4S_4 cluster[6] allows the cofactor to deliver electrons at potentials below −400 mV. The redox properties of Fe_4S_4 clusters fall into two broadly functional classes: (1) negative +2/+1 redox couples (−250 to −650 mV), typical of ferredoxins, and (2) positive +3/+2 redox couples (+50 to +450 mV), typical of the high potential iron−sulfur proteins (HiPIPs) (Backes *et al.*, 1991). In ferredoxins as compared to HiPIPs, increased exposure to solvent and more hydrogen bonds from local protein amide linkages are thought to stabilize the reduced state of the Fe_4S_4 +2/+1 redox couple (Backes *et al.*, 1991). In SiRHP, the Fe_4S_4 cubane is only 5.1 Å from the solvent-accessible surface. Although the cubane itself is completely sequestered by the surrounding ligating loops, direct cluster solvation is possible as one of the thiolate ligands, Cys479 Sγ, presents 7.7 $Å^2$ of exposed surface area. Like low-potential ferredoxins, the SiRHP protein hydrogen-bonds extensively to the Fe_4S_4 cluster (Figure 3): six of eight hydrogen bonds are supplied by main-chain nitrogens and two are supplied by side chains (sequence-variable Thr477, and conserved Asn481, which is replaced by Arg in the related assimilatory nitrite reductases). However, recent computational studies (Stephens *et al.*, 1996) stress that the redox potentials of iron−sulfur proteins are determined by a complex interplay of factors including solvent accessibility, the proximity of charged residues, and both short- and long-range dipole interactions supplied by the peptide backbone's amino and carbonyl groups. In SiRHP, the low-potential +2/+1 redox couple of the Fe_4S_4 cluster is likely stabilized by many different structural features including the coupled siroheme and its participation in a complex hydrogen-bond network that integrates the cofactors with positively charged residues in the distal anion binding site.

(C) Asymmetry of the Fe_4S_4 Cluster. Although the SiRHP Fe_4S_4 cluster conforms well with standard Fe_4S_4 geometry overall (see below), it appears to be subtly asymmetric, with at least one Fe−Fe distance involving the cubane iron bound to bridging ligand Cys483 (Fe4) being significantly shorter than the others (Crane & Getzoff, 1997). Both unrestrained conventional crystallographic refinement to 1.6 Å resolution and full-matrix least-squares refinement against multiwavelength anomalous differences to 2.5 Å resolution indicate that the Fe1−Fe4 distance (2.7 Å) is the shortest (Crane & Getzoff, 1997). All other interiron distances are quite similar to one another and are ∼0.1 Å longer than the Fe1−Fe4 separation. Although there is a slight apparent compression along one dimension of the cubane, typical of D_{2d} distortions seen in other Fe_4S_4 systems (Backes *et al.*, 1991), the shorter Fe1−Fe4 distance deforms the cluster further toward C_{2v} symmetry. The decreased Fe1−Fe4 separation could be a consequence of the unique protein environment that packs the cluster up against siroheme's proximal face and/or electronic effects of the asymmetric linkage to the siroheme iron. An inductive flow of electron density from the cluster through the cysteine thiolate bridge to the ferric siroheme iron could alleviate the π-antibonding character of Fe−S cluster bonds (Noodleman & Case, 1992), decrease the Fe1−Fe4 separation, and stabilize the electron-rich $[Fe_4S_4]^{2+}$ cluster. With 1.6 Å resolution diffraction data, the Cys483 Sγ−Fe4 bond does refine unrestrained ∼0.05 Å shorter than the other cysteine thiolate−cubane iron bonds (Table 2).

Subtle cubane asymmetry and somewhat unusual torsion angles for the cysteine-to-cubane bonds may explain spectroscopic signatures of asymmetry in the SiRHP cluster. Although the SiRHP cluster vibrational frequencies are similar to those of trigonal Fe_3S_4 clusters and therefore suggest that the cubane iron bound to the bridging thiolate may be in a unique geometry that imparts an approximate C_{3V} symmetry (Madden *et al.*, 1989), the refined Sγ−Fe−μS angles for Cys483 match those of the other SiRHP cluster ligands (Table 2) and those found in ferredoxins and HiPIPs [typical values of ∼102°, ∼114°, ∼120° from a survey of structures in the Protein Data Bank (Bernstein *et al.*, 1977)]. Terminal Fe−Sγ vibrational modes, observed above 320 cm^{-1} by resonance Raman spectroscopy, are influenced by distortions of the cubane and constraints imposed by the protein environment (Czernuszewicz *et al.*, 1987,Han *et al.*, 1989a, Backes *et al.*, 1991). In SiRHP, these modes (Fe−S^t, of symmetry B_2 and E under a D_{2d} description) exhibit large splittings and high frequencies (Madden *et al.*, 1989) characteristic of either a substantial distortion from tetrahedral (T_d) symmetry, which is not structurally apparent, or Fe−

[5] For the low molecular weight, assimilatory SiR from *D. vulgaris*, an exchangeable sulfide, reported to persist throughout reduced states and during catalysis, may act as a bridging ligand (Tan & Cowan, 1991). Perhaps the absence of a glycine at position 482 (SiRHP numbering) precludes both cysteines of the second cluster loop from simultaneously acting as ligands.

[6] In the oxidized SiRHP Fe_4S_4 cluster, each iron is formally +2.5 and each inorganic sulfur is formally −2.0, giving the cubane a conventionally referred to charge of +2. However, the formal charge on the entire cluster moiety, including thiolate ligands, is −2.

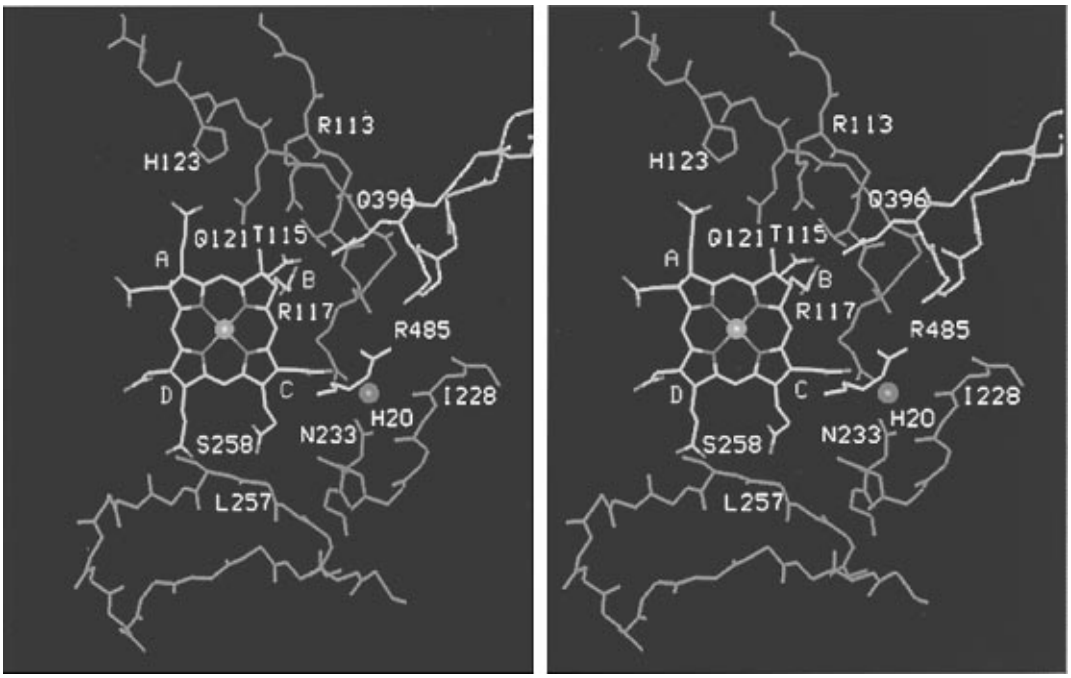

FIGURE 4: Siroheme binding pocket. Stereoview of the siroheme binding cavity viewed from the position of the Fe_4S_4 cluster with the distal ligand binding site behind and not shown. The regions shown are depicted as white in Figure 1A and the orientation is rotated ~90° about a vertical axis relative to Figure 1A. The β-strands adjoining the subdomain 1 harness turn (main chain, cyan, top) allow alternating side chains (green) to be directed for hydrogen-bonding to the siroheme carboxylate groups (Arg113 and Thr115 to ring B, Arg117 to ring C, Gln121 and His123 to ring A). Gln396 (yellow), which hydrogen bonds to pyrroline ring B (for siroheme nomenclature see Figure 2), is the only residue from the subdomain 1′ harness turn (main chain, magenta, top) that contributes to siroheme binding. A sequestered water molecule (blue sphere) couples the N-terminal spiral connection to the siroheme and its ligands by bridging the Asn233 amide, the Ile228 peptide carbonyl, and the Arg117 guanidinium and the ring C acetate through hydrogen bonds. Arg 485 from the C-terminal spiral connection interacts with a siroheme carboxylate and both harness turns. Additional interactions between the protein and siroheme are made above and below the plane of the picture. The figure was produced with AVS.

Sγ−Cβ−Cα torsion angles near 180° (Backes *et al.*, 1991). SiRHP has two torsion angles near 180° (Table 2) and splittings with frequency shifts greater than those of ferredoxins (one angle near 180°) and considerably greater than those of HiPIPs (no angles near 180°). The resolution of four distinct cluster iron sites resolved by ^{57}Fe ENDOR when the two-electron reduced enzyme is treated with small amounts of chaotropic agents (Cline *et al.*, 1986) perhaps indicates the underlying asymmetry of the Fe_4S_4 cluster asymmetry observed in the SiRHP crystallographic structure.

(D) Recognition of a Conformationally Distorted Siroheme. The siroheme is bound in a deep pocket at the interface of the three SiRHP domains (Figure 1A). Complementary van der Waals contacts and hydrogen bonds are supplied by residues from two symmetry-related "harness turns" between β3 (β3′) and β4 (β4′) of the parachute domain (Crane *et al.*, 1995), the N-terminal ends of β5 and β6 and the extended hairpin between β 8 and β 9 in domain 2, both cluster-coordinating loops in domain 3, and the symmetry-related "spiral connections" between β6 (β6′) and β7 (β7′) (Figure 4). The siroheme carboxylates form direct and water-mediated hydrogen bonds that bridge elements of protein structure to stabilize and orient the parachute domain and substrate binding site with respect to the two cluster loops. Bridging interactions mediated by siroheme carboxylates include the Asn116 peptide nitrogen, located on the harness turn, and the Val435 peptide nitrogen, located on the $CysX_5$ Cys cluster binding loop, both hydrogen-bonding to the acetate group of pyrroline B, and the side chains of His123, Gln121, and Thr489, all hydrogen-bonding to the propionate on pyrroline A. A water molecule, completely sequestered from bulk solvent, bridges the ring C acetate to the Asn233 amide, the Ile228 peptide carbonyl, and the Arg117 guanidinium, thereby involving the N-terminal spiral connection in siroheme binding. Lys306 and Lys308 on $\alpha 5_a$ interact with pyrrole rings C and D through ordered solvent and the propionates on these two rings are themselves bridged by a water molecule. The acetate of siroheme ring D participates, via a water molecule, in a hydrogen-bonding network involving Asn481, on the second cluster loop, and Arg214, at the beginning of β6. The covalent linkage between the siroheme iron and Cys483, as well as direct side-chain-to-main-chain hydrogen bonds between the parachute domain harness turns and the $CysX_3Cys$ cluster loop, further integrate the association of the N- and C-terminal SNiRRs to assemble the active center prosthetic groups and substrate binding site.

The siroheme itself is bound in a distinctive ruffled conformation that imparts S_4 point symmetry. Similar but less pronounced distortions have been observed in the crystal structures of metalloisobacteriochlorins (Kratky *et al.*, 1985, Suh *et al.*, 1984). Large dihedral angles between opposite pyrrole/pyrroline rings (Table 3) pucker the isobacteriochlorin so that the meso carbons CHB and CHD are directed down toward the cluster, while CHA and CHC are directed up toward the distal anion-binding site (Figure 2). The non-planarity of the saturated pyrroline rings, evident in their internal torsion angles (Table 3), allows their attached carboxylates to be quite axial and project above and below the plane of the ring to hydrogen-bond with the protein, bound phosphate, and ordered water molecules. In particular, the propionate on ring B, which extends toward β5 and β6 (Figure 5) and interacts with the peptide nitrogen of Asn[154]

Table 3: Refined Siroheme Coordination Geometry for HP−PO_4

Siroheme Ligand Geometries,[a] Refinement 1−3	distance (Å)		
P−O1	1.54	1.53	1.53
P−O2	1.75	1.72	1.72
P−O3	1.47	1.48	1.51
P−O4	1.54	1.54	1.53
SFe−O1	1.84	1.86	1.85
	bond angle (deg)		
SFe−O1−P	134.5	136.0	136.0

Siroheme Macrocycle Torsional Parameters[b]					
opposite ring torsions[c] (deg)		adjacent ring torsions[d] (deg)		internal ring torsions[e] (deg)	
A−C	29.9	A−B	−1.9	A pyrroline	−31.3
B−D	−28.4	B−C	2.9	B pyrroline	29.0
		C−D	−2.6	C pyrrole	−0.2
		D−A	−1.6	D pyrrole	3.8

[a] In the absence of intermolecular restraints and presence of mild internal restraints, the phosphate (1.6 Å data) orientation and geometry converged from three initial test conformations, each deviating ∼0.3 Å in individual atomic positions (refinement 1−3). Whether the internal restraints were absent, set equal, or permuted around the anions, the asymmetries were always preserved (P−O2 bond ∼0.2 Å longer than the other phosphate P−O bonds). [b] During refinement, siroheme bond lengths and angles were restrained to avoid small but unrealistic geometric distortions in pyrrole ring D. Siroheme ring planarity and internal torsion angles were unrestrained. [c] Angle between opposite pyrrole/pyrroline rings I and J of the siroheme macrocycle calculated as the average of ω(C1I−NI−NJ−C4J) and ω(C4I−NI−NJ−C1J). [d] Angle between adjacent pyrrole/pyrroline rings I and J of the siroheme macrocycle calculated as the torsion angle ω(C4I−NI−NJ−C1J). [e] Internal pyrrole/pyrroline ring I angle defined as ω(C1I−C2I−C3I−C4I).

through a bridging structural water molecule, is important for direct, side-chain mediated, and water-mediated contacts with distally coordinated anions (Figure 4).

The SiRHP cofactors seem well suited for stabilization of a siroheme π-cation radical and thus the provision of an additional reducing equivalent. In the reduction of nitrite to ammonia, a three-electron step exists between two stable intermediates, nitric oxide (NO) and hydroxylamine (NH_2 OH); thus, delivery of three electrons from enzyme to substrate, in rapid succession, may reduce the necessity of stabilizing the intervening species. Isobacteriochlorins have destabilized HOMO a_{1u} orbitals due to the reduced delocalization caused by the saturated pyrroline rings (Chang *et al.*, 1981). The reduction potentials for free, metallated, and complexed isobacteriochlorin π-cation radicals are 200−300 mV lower than for their chlorin counterparts and up to 500 mV lower than their porphyrin counterparts (Young & Siegel, 1988a; Fujita *et al.*, 1985; Fujita & Fajer, 1983, Chang & Fajer, 1980). When treated with the oxidizing agent porphyrexide, SiRHP will form a stable siroheme π cation (Young & Siegel, 1988a). The deviation from planarity caused by the extensive S_4 ruffling of the SiRHP siroheme would further destabilize the HOMO orbital and increase the efficacy of oxidizing the ring. Charge transfer into the macrocycle π* orbitals from the closely juxtaposed electron-rich Fe_4S_4 cluster, through the covalent sulfur bridge and/or the van der Waals contact, could help stabilize a tetrahydroporphyrin cation species. Downshifts seen by resonance Raman in the in-plane vibrational modes of the protein-bound siroheme are expected for the observed S_4 ring deformation, sixth axial ligand, and possible charge transfer into the macrocycle π* oribitals (Madden *et al.*, 1989). The latter is also consistent with the observed cluster asymmetry.

(E) A Distal Heme Pocket Optimized To Bind Anions. As isolated and crystallized, SiRHP binds a phosphate in the distal anion binding site through a 1.85 Å Fe−O bond to the high-spin ($S = {}^5/_2$) ferric siroheme iron. The siroheme Fe−O−P angle (Table 3), indicative of a σ-bonding interaction between the iron and phosphate lone pair, is consistent with the geometry of sulfate anions bound to model isobacteriochlorins (Reynolds & Holm, 1989). The ruffled conformation of the isobacteriochlorin ring produces a larger core size to accommodate the large, high-spin, ferric iron with less displacement above the least-squares plane of the pyrrole/pyrroline nitrogens (0.29 Å) than the usual 0.39−0.54 Å found in ferric high-spin porphyrin complexes (Scheidt & Reed, 1981). In analogy to sulfate or nitrate, phosphate should be a relatively weak field axial ligand (Scheidt & Reed, 1981). Five-coordinate heme complexes with typical ∼2.3 Å iron−thiolate bonds are usually high-spin but can become low-spin on the addition of a sixth axial ligand (Collman *et al.*, 1977; Raag & Poulos, 1989). The high-spin state of the six-coordinate ferric siroheme in SiRHP is presumably promoted by phosphate being a weak-field ligand, a long bond between the siroheme Fe and the axial Cys483 thiolate, and the covalent coupling of this same thiolate to the Fe_4S_4 cluster.

In the active center of HP−PO_4 the phosphate is tightly coordinated by extended positively charged side chains (Figures 1B and 5), supplied from β1 (Arg83), β5 (Arg153),[7] and β 6 (Lys215 and Lys217).[8] The entire active-site cleft is highly solvated by ordered water molecules, which form complicated hydrogen-bond networks between the siroheme carboxylates, charged active-site residues, and bound phosphate. The channel from solvent to the substrate binding site is shaped on one side by the siroheme, which directs the acetate groups attached to C2A and C3D (Figures 1B and 2) into bulk solvent, and on the other side by the four ligand-binding residues, Arg83, Arg153, Lys215, and Lys217 (Figure 5). The active-site channel allows solvent accessibility to only one phosphate oxygen (O4), which forms a strong hydrogen bond of 2.7 Å with an exposed ordered water molecule (Figure 5) This exposed water molecule itself interacts with a layer of ordered water molecules that lines the channel's mouth and surface of the surrounding protein (Figure 1B). As the active-site cleft broadens and becomes shallow beyond the edge of the siroheme and ligand-binding residues, it is flanked by β1, the partially disordered loop between α2 and β5, and the $CysX_5Cys$ cluster-binding loop, which juxtaposes the exposed siroheme acetate groups. Thus, the ligand binding site is relatively close to the surface of the molecule and is not occluded by surrounding protein loops. However, the active-site side chains can tightly ensconce bound anions against the face of the siroheme and thereby allow minimal exposure to solvent.

[7] On the basis of alignment of the four SNiRR homology regions proposed in Crane *et al.*, (1995), His86 of the low molecular weight assimilatory SiR from *D. vulgaris* is analogous to SiRHP Arg153. In the *D. vulgaris* enzyme, His86 might bind directly to the siroheme in the absence of a bound anion, accounting for the histidine proximal ligand implicated by hyperfine-shifted NMR (Cowan & Sola, 1990).

[8] Lys215 NZ to siroheme ND = 3.60 Å, Lys215 NZ to center of ring D = 3.24 Å, Lys217 NZ to siroheme NC = 3.57 Å, and Lys217 NZ to center of ring C = 3.00 Å. The effect of having two positively charged lysine residues in contact with the pyrrole rings on forming a siroheme π-cation radical might warrant attention.

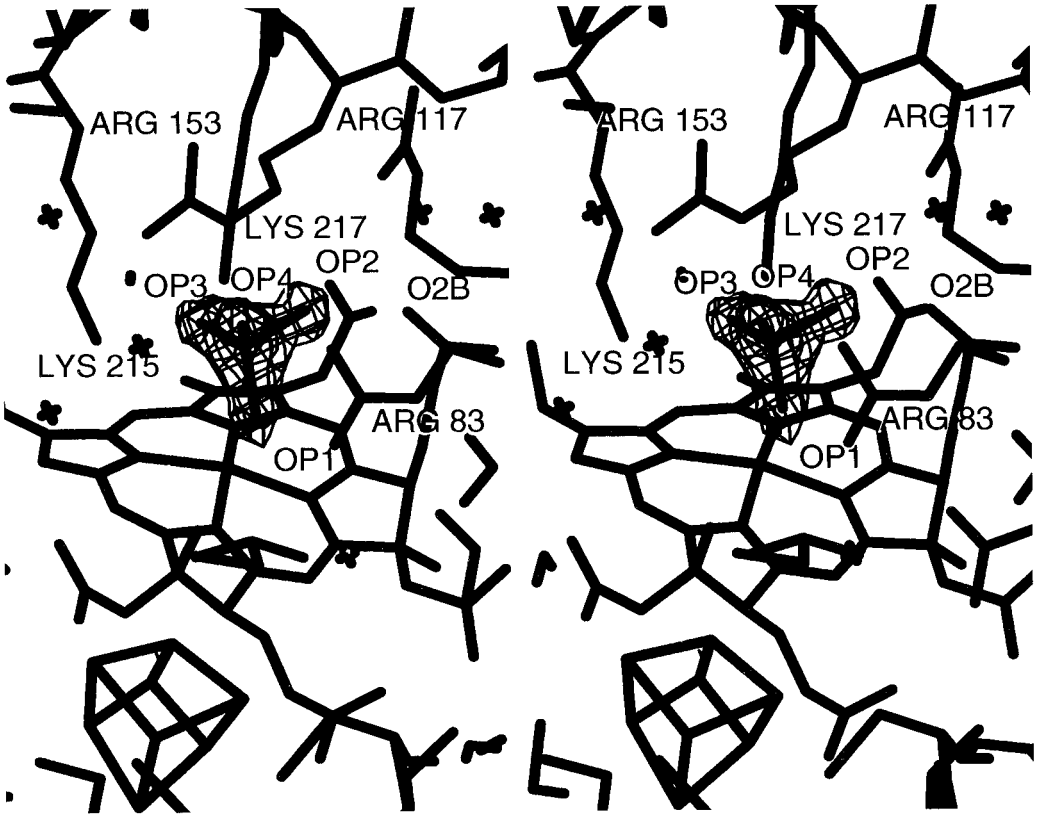

FIGURE 5: Stereoview of electron density for phosphate bound in the active site of oxidized SiRHP. Electron density contoured at 8σ in a 1.6 Å resolution $F_o - F_c$ omit map, calculated without phosphate contributing to F_c, shows that phosphate binds to the ferric siroheme iron through OP1 and is coordinated by Arg83, Arg153, Lys215, Lys217, a solvent-exposed water molecule (cross in foreground to the left of phosphate) and the most axial propionate of the siroheme's pyrroline ring B (oxygen O2B). Slight asymmetry in the tetrahedral difference density peak indicates that the bond between phosphorus and OP2 is longer than the bonds to the other phosphate oxygens (Table 3). OP2 is likely protonated, as it is also in hydrogen-bonding distance to the axial propionate of pyrroline ring B. Positional refinement of the model without phosphate was carried out for 40 cycles with X-PLOR before calculation of the omit map. The figure was rendered with XFIT (McRee, 1992).

In the SiRHP structure, determined at pH 7.7, the phosphate appears singly protonated (HPO_4^{2-}) as one P−O bond refines ~0.2 Å longer than the others (Table 3) and the oxygen (O2) of this bond is in hydrogen-bonding distance (2.7 Å) to the axial propionate of siroheme pyrroline ring B. Over a pD range of 6.0−9.9, a hyperfine-shifted NMR resonance tentatively assigned as a pyrroline propionate α-CH exhibits a 10 ppm shift, too large for protonation of the carboxylate itself without substantial structural rearrangement (Kaufman *et al.*, 1993a). Conversion between $H_2PO_4^-$ and HPO_4^{2-} is the most likely deprotonation event, given the ionizable groups present in the active site and the pH range involved. Although the pK_as of Lys^{215} and Lys^{217} may be perturbed by the active center's high charge density, these residues extend toward the unsaturated side of the isobacteriochlorin and away from the pyrroline rings, while the phosphate is close to the axial siroheme propionate (Figure 5).

Interaction of SiRHP with Phosphate in Solution. In solution, the oxidized form of SiRHP binds phosphate tightly in its active center; however, the anion is readily released on reduction of the cofactors. Figure 6 shows binding of [^{32}P] phosphate to oxidized SiRHP after electrophoresis of the complex into a nondenaturing polyacrylamide gel at pH 7.7. After incubation of 1.6 μM enzyme with increasing concentrations of $H^{32}PO_4^{2-}$ for 24 h, partial binding is observed with 8 μM $H^{32}PO_4^{2-}$ and saturation occurs at less than 80 μM. The observed binding of $H^{32}PO_4^{2-}$ was completely competed by 100 μM HSO_3^-, indicating that phosphate is indeed binding to the siroheme on its distal face. At

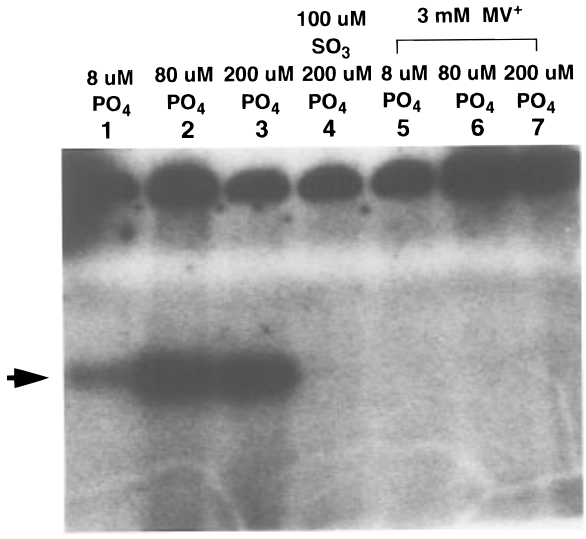

FIGURE 6: Electrophoresis of SiRHP and $K_2H^{32}PO_4$ under nondenaturing conditions demonstrates that, in solution, oxidized SiRHP binds phosphate in its active center, whereas reduced SiRHP does not. Oxidized SiRHP (1.5 μM) was incubated with $K_2H^{32}PO_4$ for 24 h at 25 °C in 100 mM HEPES, pH 7.7, before 6 μL aliquots of the assays were loaded and run on a 4−20% gradient acrylamide gel in Tris/glycine, pH 7.7 (see Experimental Procedures). Gels were dried and exposed overnight to X-ray film. For lanes 5−7, the reducing agent MV^+ was added immediately prior to loading the samples onto the gel.

concentrations of radiolabeled phosphate below 100 μM no binding to the oxidized enzyme was observed by gel analysis when incubation times were less than 15 min, indicating that equilibrium must be established over a period at least greater than this. The reduction of SiRHP with 3 mM MV^+ prior to electrophoresis completely abolishes binding of $H^{32}PO_4^{2-}$ at concentrations from 8 to 200 μM (Figure 6). MV^+ can be used to supply reducing equivalents for kinetic assays of SiRHP activity (Krueger & Siegel, 1982) and at 3 mM will completely reduce both the siroheme and Fe_4S_4 cluster. It was expected that some reoxidation of reduced samples would occur during electrophoresis, but due to slow association rates, the re-oxidation of SiRHP was not accompanied by appreciable phosphate binding. When the time of incubation was increased from a few minutes to 24 h, no binding of phosphate to the reduced enzyme was observed, indicating that at equilibrium the two-electron reduced state of the enzyme does not appreciably bind phosphate and that phosphate release on reduction is not dependent on transiently occupying the one-electron reduced state. Structures determined from SiRHP crystals soaked in millimolar concentrations of MV^+ reveal no detrimental structural effect of the reagent on the enzyme and no specific binding site for MV^+ (data not shown).

A relatively slow rate constant for the association of phosphate and SiRHP justified determination of the K_D for SiRHP and phosphate by a fast filtration method where free $H^{32}PO_4^{2-}$ was separated from SiRHP-bound $H^{32}PO_4^{2-}$ by rapidly centrifuging incubated assay fractions through a Microcon filter. Since no binding to the oxidized enzyme of radiolabeled phosphate at concentrations below 100 μM was observed over intervals less than 15 min, changes in ligand concentration during the 2 min of rapid centrifugation should not substantially perturb the fraction of phosphate bound. As described in Experimental Procedures, competition binding assays of cold HPO_4^{2-} with two fixed concentrations of hot $H^{32}PO_4^{2-}$ were used to determine a K_D of 14 $\pm$ 1 μM for phosphate and oxidized SiRHP at pH 7.7 (Figure 7). Although the gel experiments are not performed under equilibrium conditions, the binding and saturation behavior of phosphate depicted in Figure 6 also agrees well with a K_D of 14 μM.

Structures of SiRHP from Crystals Treated with Reducing Agents. Crystals of reduced SiRHP were generated from anaerobically grown crystals of oxidized protein either by soaking in millimolar concentrations of Cr(II) EDTA or by photoreducing crystals soaked in proflavin/EDTA solutions (Table 4). Obtaining the two-electron reduced state of SiRHP, where the siroheme is formally Fe^{2+} and the iron−sulfur cluster is $Fe_4S_4^{1+}$, was difficult in the crystalline state. Complete reduction required hours of soaking in high concentrations of Cr(II) EDTA, yet too high concentrations caused damage to the prosthetic groups. Crystals soaked for up to 16 h in concentrations of Cr(II) EDTA that were less than 10 mM always retained orientation-dependent EPR signals characteristic of $S = {}^5/_2$ ferric iron, indicating incomplete reduction, while crystals soaked in fresh solutions of ≥10 mM Cr(II) EDTA became bleached, lost the ability to diffract, and produced large, orientation independent EPR signals at $g = 4.3$, characteristic of free ferric iron. SiRHP crystals were more stable in 10 mM Cr(II) EDTA solutions that had been prepared at least 12−14 h previously and had thus oxidized to some extent. In the diffraction experiments

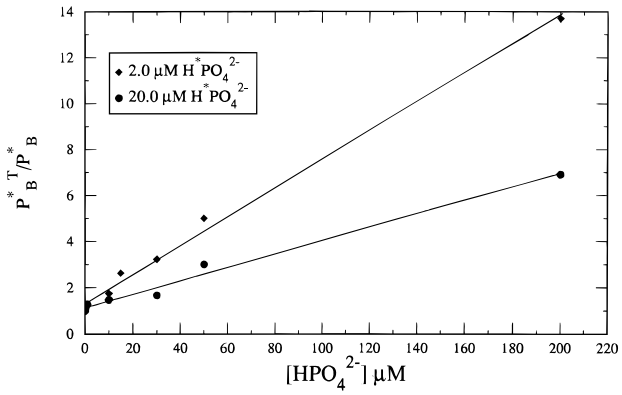

FIGURE 7: Determination of a 14 μM dissociation constant of SiRHP and phosphate by competing cold micromolar K_2HPO_4 with micromolar $K_2H^{32}PO_4$ and then rapidly separating bound ligand by filtration. The ratio of $H^{32}PO_4^{2-}$ bound with no cold HPO_4^{2-} present ($P^*_B{}^T$) to the concentration of $H^{32}PO_4^{2-}$ bound in the presence of competing cold HPO_4^{2-} (P^*_B) is plotted versus the concentration of cold HPO_4^{2-} at two fixed concentrations of $K_2H^{32}PO_4$ (2 and 20 μM). The slope of each line is equal to the concentration of cold phosphate that will displace half of the bound radiolabeled phosphate at each fixed value of P^* or $P^* + K_D$ (see Experimental Procedures). Fitting two straight lines to the data and solving two equations in two unknowns leads to a $K_D = 14 \pm 1$ μM and a value of P^* of 2.0 μM for the lower concentration. This calculated concentration of $H^{32}PO_4^{2-}$ agrees well with the value of 1.9 μM determined by direct counting of the assay cocktails prior to filtration.

reported here (Tables 1 and 4), crystals were treated with 24-h-old Cr(II) EDTA solutions. All attempts to grow crystals from protein that had already been reduced by photoreduction, MV^+, or Cr(II) EDTA were unsuccessful. Micro- and macroseed crystals of oxidized SiRHP placed into drops containing reduced protein together with varied concentrations of potassium phosphate and the crystallization agent PEG 8K failed to grow anaerobically but grew when exposed to air.

Crystallographic characterization of SiRHP under reducing conditions established that the bridging thiolate remains bound to the siroheme in all reduced states of the enzyme and verified that reduction of the protein can lead to release of phosphate from the substrate-binding site, although phosphate remains bound when present at high concentrations. EPR signals from the oxidized high-spin siroheme were absent when crystals in 65 mM phospate buffer were treated with Cr(II) EDTA in a manner most likely to achieve full reduction of both prosthetic groups (Figure 8A, top trace), but these signals were recovered when the crystals were exposed to air (Figure 8A, bottom trace). Reduction of the siroheme by Cr(II) EDTA also implies reduction of the cluster because the two prosthetic groups are electronically and covalently coupled and the redox potential of the Cr(II) EDTA reagent is far below that of the SiRHP Fe_4S_4 cluster (by at least 600 mV). The structure of SiRHP from crystals reduced with Cr(II) EDTA in the presence of phosphate (HP−PO_4 CrII, Tables 1 and 4) is very similar to the structure of the oxidized enzyme except for small correlated decreases (<0.2 Å) in the distances from SFe to Cys^{483} Sγ and to the closest cluster iron (Fe4), as well as decreases in the doming of the siroheme iron and in the average metal−ligand bond length between the siroheme iron and the pyrrole or pyrroline nitrogens (⟨N_p−SFe⟩, Tables 5 and 6). Phosphate remains bound in the active site at high occupancy. In contrast, when SiRHP crystals are treated with

Table 4: Conditions for Reducing SiRHP Crystals

structure	buffer condition	reductant	time of reduction[a] (min)	crystal size (mm^3)	phosphate occupancy
HP−PO_4	65 mM KP_i, pH 7.7			1.0 × 0.2 × 0.2	1.0
HP−PO_4 CrII	65 mM KP_i, pH 7.7	10 mM Cr(II) EDTA	30[b]	0.7 × 0.2 × 0.15	1.0
HP−PO_4 PR1	65 mM KP_i, pH 7.7	0.75 mM proflavin and 50 mM EDTA	50	0.6× 0.15× 0.08	1.0
HP−PO_4 PR2	65 mM KP_i, pH 7.7	0.75 mM proflavin and 10 mM EDTA	20	1.2× 0.2× 0.15	0.5
HP_{Em} CrII	130 mM HEPES, pH 7.7	10 mM Cr EDTA	20	0.4× 0.1× 0.08	0.0

[a] Time duration crystals were immersed in 100 μL of the Cr(II)(EDTA) reductant buffer or were irradiated with a fiber-optic light source for photoreduction. Crystals were stabilized by 15% PEG 8K. [b] Crystal was stored surrounded by <10 μL of reductant in a sealed capillary during the 20 h until data collection. All diffraction data was collected at SSRL beam-line 7-1 over a period of ~ 4.5 h.

Cr(II) EDTA for 20 min in the absence of phosphate, the resulting crystal structure (Figure 9) contains no bound phosphate in the active site (HP_{Em} CrII, Tables 1 and 4). Release of phosphate from the active center must be dependent on reduction of the prosthetic groups because, in the absence of an exchangeable ligand, phosphate will remain in the active site of oxidized SiRHP even after the crystals have been soaked for over a week in HEPES/PEG without phosphate (crystallographic data not shown).

As shown by the HP_{Em} CrII structure, the absence of a bound ligand results in considerable disorder in the positively charged side chains of the distal pocket (Figure 9). Without a ligand to stabilize the positively charged active-site side chains, the electron density for Arg83, Arg153, and Lys215 is weak, Lys215 resides in two conformations, and the thermal factors for all of these residues are much higher than in structures with ligands bound (Crane *et al.*, 1997b). Although the siroheme does not have a sixth aquo ligand, there is electron density for a buried water molecule at the back of the distal pocket, in the same position that a water molecule is found in the sulfite complex (Crane *et al.*, 1997b). In the empty, reduced active center of HP_{Em} CrII, the siroheme iron has moved completely into the plane of the pyrrole and pyrroline nitrogens, decreasing the distance between SFe and Cys483 S^{γ} to 2.4 Å (Table 5) and the distance between SFe and the closest cluster iron to 4.1 Å. Thus, in the HP_{Em} CrII structure, the siroheme iron is not domed, suggesting that the radius of SFe is small, the $d_{x^2-y^2}$ orbital is unoccupied, and the pentacoordinate siroheme iron is likely either of low or intermediate spin.

By employing a photoreduction system, we attempted to crystallographically characterize an intermediate reduction state of SiRHP in which the most populated oxidation state has a formally reduced Fe^{2+} siroheme and a formally oxidized $Fe_4S_4^{2+}$ cluster. The similarity for the reduction potentials of the siroheme (−340 mV) and the Fe_4S_4 cluster (−405 mV) and their covalent linkage prevents full occupancy of the state where only the siroheme is reduced at equilibrium. On titration of SiRHP in solution with reducing agents, the population of the one-electron reduced species (HP −1) maximizes at ~0.5 of the total enzyme molecules present when the oxidized (HP) and fully reduced species (HP −2) are approximately equally occupied at 0.25 each. Loss of the ferric siroheme EPR signals from crystals soaked in a flavin/EDTA solution was dependent on time of irradiation with visible light and was reversible with reoxidation (Figure 8B,C). Structures from crystals photoreduced for different lengths of time (HP−PO_4 PR1 and HP−PO_4 PR2) revealed variations in the occupancy of the bound phosphate. There was no change in phosphate occupancy for crystals soaked in proflavin/EDTA but not irradiated, nor for crystals reduced by irradiation but then reoxidized by air exposure prior to data collection. Extensive photoreduction in the presence of 65 mM phosphate for a period of time sufficient to abolish the high-spin iron EPR signals (Figure 8C) resulted in a structure (HP−PO_4 PR1) much like the structure after reduction with Cr(II) EDTA (HP−PO_4 CrII). The most distinctive differences between the extensively photoreduced crystal HP−PO_4 PR1 and the oxidized enzyme (Tables 5 and 6) are again a small movement of the siroheme iron into the plane of the macrocycle for HP−PO_4 PR1 and a decrease in $\langle N_p-SFe\rangle$. The distance between Cys483 Sγ and the siroheme iron in HP−PO_4 PR1 is 2.7 Å, which compares to the values for HP−PO_4 CrII of 2.7 Å and HP−PO_4 of 2.8 Å.

Photoreduction for periods of time shorter than the treatment for HP−PO_4 PR1 only attenuated, but did not abolish, the high-spin iron EPR signals (Figure 8B) and produced a structure with decreased phosphate occupancy (HP−PO_4 PR2), even though the *in situ* phosphate concentration remained high at 65 mM. In the intermediately photoreduced crystal HP−PO_4 PR2, both the phosphate bound in the active site and a water molecule at the mouth of the active-site channel that hydrogen bonds to phosphate oxygen OP4 were at much lower occupancy than in the oxidized enzyme or in any other of the reduced state structures (Figure 10; and see Figure 5 for phosphate nomenclature). The $F_o - F_c$ difference Fourier calculated between HP−PO_4 CrII and HP−PO_4 PR2 (Figure 10A) presents a large positive peak at the position of the phosphorus and distal oxygens of phosphate, as well as negative density closer to the siroheme, indicating reduced occupancy of phosphate and the presence of a smaller siroheme ligand in the HP−PO_4 PR2 structure compared to the HP−PO_4 CrII structure. The SiRHP model was refined against the HP−PO_4 PR2 diffraction data with successively decreasing occupancies for phosphate. $F_o - F_c$ difference maps were examined to find the value of phosphate occupancy that would completely remove the electron density due to the phosphate phosphorus, the phosphate distal oxygen atoms, and the interacting, exposed water molecule. Thermal factors for phosphate and the exposed water molecule were set equal to values found in the oxidized structure, after those values had been scaled by the ratio of the average protein thermal factors between the two structures. With the phosphate occupancy set to 0.5, the phosphate density was removed from the $F_o - F_c$ difference maps and only a spherical density peak approximately 2.0 Å to the distal side of the siroheme iron remains (Figure 10B). Thus, in the secondary species composing the HP−PO_4 PR2 crystal, a water or hydroxide molecule, instead of phosphate, may bind the siroheme iron. The HP−PO_4 PR2 structure was refined

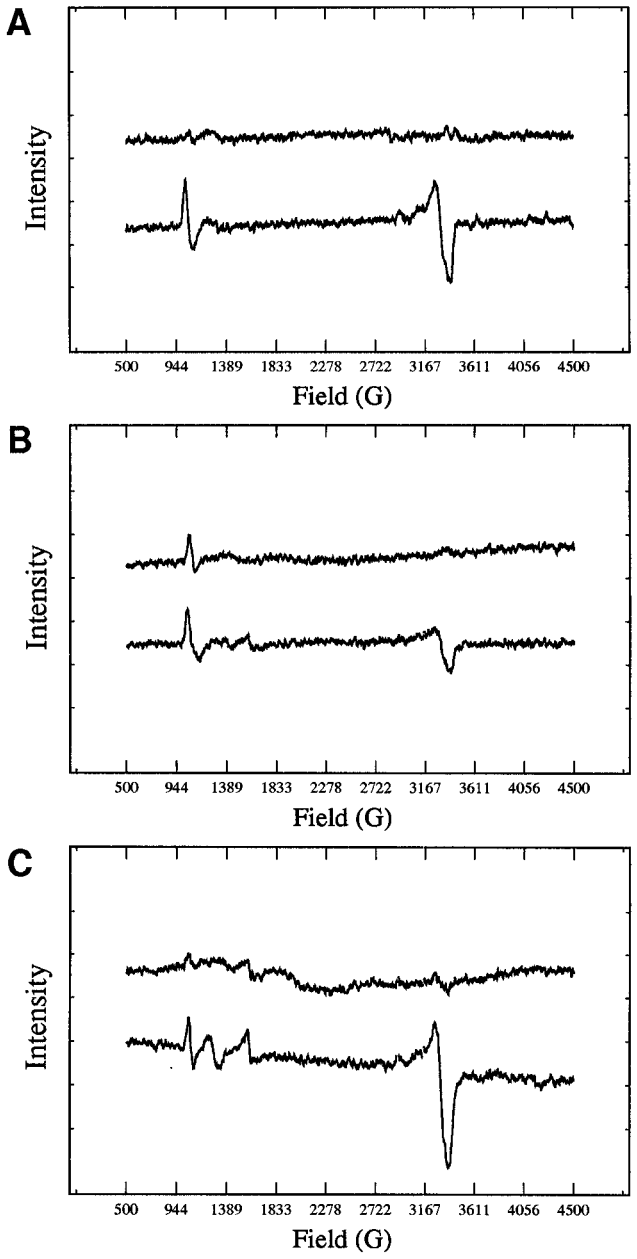

FIGURE 8: Single-crystal EPR spectra monitoring SiRHP oxidation state. (A) EPR spectra measured at 9 K on a crystal soaked for 12 h in a 10 mM Cr(II) EDTA/KP_i/PEG solution that was a day old and partially oxidized, before (upper trace) and after (lower trace) exposure to air, indicate complete reduction at the siroheme. Reoxidation of the sample by blowing air into the EPR tube for 20 min at 298 K results in the appearance of a low-field signal characteristic of ferric high-spin ($S = {}^5/_2$) siroheme iron (shown at an orientation that gives $g = 6.28$ or 1082 G). The signal that appears at $g = 2.03$ (3350 G) is independent of the orientation of the sample and is likely caused by contamination with copper (Cu^{2+} is only present on reoxidation). Spectra were corrected for background by subtracting the spectrum of an empty EPR tube. Gain $= 8 \times 10^5$. (B) EPR spectra measured at 9 K (see Experimental Procedures) on a single SiRHP crystal irradiated for 20 min in the presence of 750 μM proflavin and 10 mM EDTA ($HP-PO_4$ PR2, Table 1), before (upper trace) and after (lower trace) reoxidation, indicate partial reduction at the siroheme. Exposure to air increases the intensity of the low-field signal characteristic of high-spin siroheme by a factor of 2 (determined by comparing the areas of each peak after double integration). (C) EPR spectrum measured at 9 K on a crystal photoreduced for 50 min with 750 μM proflavin and 50 mM EDTA in KP_i/PEG (($HP-PO_4$ PR1, Table 1) shows little remaining high-spin siroheme signal (upper trace). Reoxidation (lower trace) results in orientation-dependent low-field signals characteristic of high-spin $S = {}^5/_2$ ferric heme. Gain $= 8 \times 10^5$.

to 1.8 Å resolution, with both a phosphate and a water molecule present at half occupancy in the active site. Although the siroheme iron position might be slightly different in the two species present in the crystal, the extent of the change was too small to be identified by refining alternate conformations for the siroheme iron. The value of $\langle N_p-SFe \rangle$ for $HP-PO_4$ PR2 (Table 5) is intermediate between those of the oxidized and the fully reduced states, which reflects the siroheme iron position of HP −1 and/or a mixture of oxidation states in the crystal. We propose that the one-electron reduced enzyme (HP −1) is partially represented in $HP-PO_4$ PR2, at an occupancy of ~0.5, and that this species binds a water molecule, instead of phosphate in its active center.

Alterations in the Fe_4S_4 cluster geometry on reduction were too small to accurately characterize even with 1.75 Å resolution diffraction data. When geometrical restraints are not placed on the Fe_4S_4 cluster during refinement, accurate separation of the cluster atoms is limited by the resolution of the diffraction data. For example, the highest resolution structure at 1.6 Å ($HP-PO_4$) has the largest average Fe−S separations, and these average separations consistently decrease as the diffraction data worsens in resolution. For diffraction data sets that do not reach 2.0 Å resolution, geometric restraints had to be imposed on the cluster geometry to prevent an unrealistic, collapsed configuration. As well, there appears to be a slight shift (0.1−0.2 Å) in the position of the active site and surrounding loops in the reduced states compared to the oxidized state.[9] Thus, difference Fourier maps between the oxidized and reduced states ($F_o - F_c$) tend to emphasize this concerted movement of the metal atoms and not changes in internal cluster geometry. However, a difference Fourier between the $HP-PO_4$ CrII data (presumed 100% HP −2) and the $HP-PO_4$ PR2 structure (presumed 50% HP −1) indicates that the cluster is expanded in the $HP-PO_4$ CrII structure, roughly along the body diagonal directed toward the bridging ligand and siroheme (Figure 10A). These difference peaks surrounding the cluster probably represent a real difference in cluster position and/or size between $HP-PO_4$ CrII and $HP-PO_4$ PR2 because $F_o - F_c$ difference maps of the individual structures, calculated with the complete refined models contributing to F_c, have few features around the metals at contour levels at or above 1σ, providing an overall anisotropic thermal factor has been applied to the diffraction data.

GENERAL CONCLUSIONS

The SiRHP protein assembles the siroheme and Fe_4S_4 cluster in a manner that enhances their joint ability to catalyze multielectron reductions of inorganic anions. Intimate association between the siroheme and Fe_4S_4 cluster by covalent bonding through the shared cysteine thiolate and by close contact allowed by the ruffled shape of the siroheme promotes electronic coupling important for catalysis. The distorted conformation of the siroheme recognized by the protein also results in axial configurations of the siroheme's propionate side chains for interaction with bound anions, active-site residues, and ordered water molecules. The reduction potential and reactivity of the Fe_4S_4 cluster may

[9] This small shift is unlikely to explain the difficulty in growing crystals from reduced protein because it is localized to the active-center region and does not disrupt packing contacts in the crystal lattice.

Table 5: Ligand and Cofactor Geometries for Various Oxidation States of SiRHP

structure[a]	S−SFe[b] (Å)	S−Fe4[c] (Å)	SFe−OP1[d] (Å)	SFe−Fe4[e] (Å)	CHB−S1[f] (Å)	SFe−S−Fe4[g] (deg)	SFe−OP1−P[h] (deg)	dome[i] SFe (Å)	⟨disp⟩[j] srm (Å)	⟨N_p −SFe⟩[k] (Å)
HP−PO_4	2.84	2.17	1.86	4.48	3.62	126.3	135.1	0.30	0.30	2.11
HP−PO_4 CrII	2.69	2.18	1.87	4.35	3.88	125.9	139.4	0.18	0.28	2.04
HP−PO_4 PR1	2.69	2.23	1.82	4.38	3.66	125.4	138.5	0.23	0.29	2.04
HP−PO_4 PR2[l]	2.68	2.21	1.85,[m] 1.96	4.35	3.63	125.6	144.0	0.24	0.32	2.07
HP_{Em} CrII	2.37	2.25		4.13	3.75	126.1		0.01	0.27	2.03

[a] See Table 1 for nomenclature and diffraction statistics of each crystal structure. [b] Bond length between the bridging cysteine thiolate of Cys483 (S) and the siroheme iron (SFe). [c] Bond length between the bridging cysteine thiolate of Cys483 (S) and the Fe_4S_4 cluster iron (Fe4). [d] Bond length between the siroheme iron and the closest atom of the exogenous axial ligand (L1). [e] Separation between the siroheme iron and closest cluster iron (Fe4). [f] van der Waals contact distance between the siroheme meso carbon CHB and the cluster inorganic sulfur S1. [g] Angle defined by the siroheme iron, bridging sulfur, and covalently linked cluster iron. [h] Angle defined by the siroheme iron, the bound oxygen of the phosphate, and the phosphorus. [i] Doming or displacement of the siroheme iron above the least-squares best plane formed by the pyrrole and pyrroline nitrogens of the siroheme. A positive displacement is in the direction of the distal-ligand binding position. [j] Average displacement of the 24 atoms in the isobacteriochlorin ring and the siroheme iron from their least-squares best plane. [k] Average separation between the siroheme iron and the pyrrole or pyrroline nitrogens. [l] This photoreduced crystal is likely of intermediate oxidation state and therefore contains a mixture of species. Thus, the refined geometric parameters represent a distribution of states, over which phosphate is only partially occupied. [m] Bond lengths are given for the SFe to phosphate oxygen (first number) and water oxygen (second number) as both ligands are present in the HP−PO_4 PR2 crystal, each at partial occupancy.

Table 6: Hydrogen-Bonding Distances and Separations between Bound Phosphate and Active-Site Residues of SiRHP in Various Oxidation States

structure[a]	Arg83[b] N1, N2 (Å)	Arg153[b] NE (Å)	Lys215[b] NZ (Å)	Lys217[b] NZ (Å)	srm[c] O2B (Å)	exp[d] H_2O (Å)
HP−PO_4	OP4 2.83	OP4 2.78	OP3 2.69	OP3 2.78	OP2 2.73	OP4 2.75
	OP1 3.53		OP4 3.65	OP2 3.49		
HP−PO_4 CrII	OP4 2.86	OP4 2.70	OP3 2.63	OP3 2.74	OP2 2.65	OP4 2.72
	OP1 3.67		OP4 3.53	OP2 3.42		
HP−PO_4 PR1	OP4 2.65	OP4 2.70	OP3 2.73	OP3 2.65	OP2 2.71	OP4 2.67
	OP1 3.58		OP4 3.50	OP2 3.46		
HP−PO_4 PR2[e]	OP4 2.73	OP4 2.52	OP3 2.47	OP3 2.78	OP2 2.69	OP4 2.41
	OP1 3.82		OP4 3.27	OP2 3.61		

[a] See Table 1 for nomenclature and diffraction statistics of each crystal structure. [b] Hydrogen-bonding distances and separations between bound ligands and the four active-site residues that contact them (Arg83, Arg153, Lys215, and Lys217). For Arg83 the hydrogen-bonding distances to the ligand atom specified in the table are given for Arg NH1 (N1), Arg NH2 (N2) in descending order, whereas for Arg153, hydrogen-bonding distance to the guanidinium NE is given. For lysine, all distances are between the specified ligand atom and Lys NZ. [c] Hydrogen-bonding distance to the siroheme's most axial propionate (oxygen O2B) on pyrroline ring B. [d] Hydrogen-bonding distance to an exposed water molecule (exp H_2O) that is positioned at the mouth of the active-site channel. [e] Phosphate at half occupancy. The water ligand bound at half occupancy to the siroheme iron is not in hydrogen-bonding distance to the phosphate ligands.

be determined in part by its association with the siroheme, by accessibility to solvent, and by hydrogen bonds to its inorganic sulfides and thiolate ligands supplied by both main-chain and side-chain functional groups within the protein loops containing the four cluster-ligating cysteines. A tightly constrained Cys^{479} X_3Cys^{483} loop positions the Cys^{483} ligand for coordination to the siroheme's proximal axial coordination site, whereas the $Cys^{434}X_5Cys^{440}$ loop forms a flap over the cluster that sequesters it from bulk solvent. Substrates and other anions are recognized by an active-site pocket distal to the siroheme that is exquisitely designed for electrophilic or general acid catalysis. Positively charged arginine and lysine residues extended from the β-strands of two domains form hydrogen-bond networks with bound exogenous ligand, the axial siroheme carboxylates, and ordered water molecules to cage exogenous ligands (Table 6).

Comparisons among structures of SiRHP in its three stable oxidation states support a structural basis for the relationship between cofactor oxidation state and the protein's ability to bind and react with ligands. Presence of a bound phosphate stabilizing the unusually high density of side-chain positive charges in the active center of the oxidized enzyme suggests that inhibition by this anion may explain the 10^5-fold slower binding rates of substrates and inhibitors compared to the reduced enzyme (Janick *et al.*, 1983), as well as the high-pH activation of SiRHP, after reduction and reoxidation in the absence of phosphate (Young & Siegel, 1988b). Reduction of the SiRHP prosthetic groups affects the interaction of siroheme with phosphate in the distal ligand-binding pocket. Crystals treated with Cr(II) EDTA in a fashion most likely to yield complete reduction of both prosthetic groups (Figure 8A) showed little change in coordination of the exogenous phosphate (Tables 5 and 6) in the presence of 65 mM phosphate; however, the exogenous phosphate anion was lost from the active center in minutes when crystals were similarly reduced in the absence of phosphate. The 2.4 Å separation between the siroheme iron and Cys483 S^{γ} and the 4.1 Å separation between the siroheme iron and Fe4 of the cluster in HP_{Em} CrII are the smallest of any SiRHP species studied crystallographically (Table 5; Crane *et al.*, 1997b), indicating that distal ligands compete strongly with the Cys483 S^{γ} for the SFe bonding orbitals. Although the siroheme in the oxidized enzyme will bind both σ-donor ligands such as phosphate and π-acceptor ligands such as sulfite, the reduced states favor strong π-acceptor ligands, such as the substrates sulfite and nitrite, over phosphate. Shorter average distances between the siroheme iron and the pyrrole or pyrroline nitrogens (⟨N_p−SFe⟩) in all of the reduced states compared to the oxidized state may destabilize the $d_{x^2-y^2}$ orbital of the siroheme iron and facilitate electron transfer to axial π-acceptor ligands.

Of the three distinct SiRHP oxidation states (HP, HP −1, and HP −2), one-electron reduced SiRHP (HP −1) may have the lowest affinity for axial siroheme ligands. In the presence

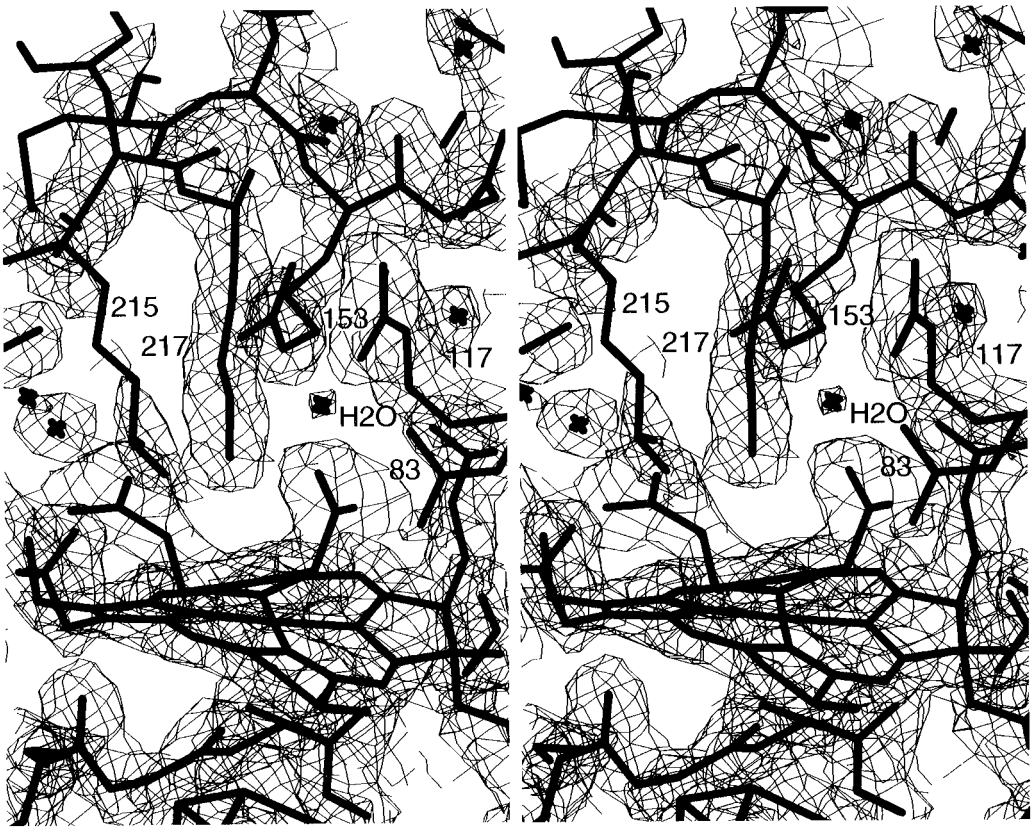

FIGURE 9: Stereoview of the HP_{Em} CrII active center with no exogenous ligands bound. Electron density contoured at 1σ and 5σ in a 2.2 Å resolution $2F_o - F_c$ map shows an empty active center where the siroheme iron has moved down into the plane of the porphyrin relative to ligated states (Table 5). There is disorder in the active-site side chains that normally coordinate ligands. The density for the side chain of Arg153 is weak and the side chain of Lys215 has two conformations. Although no water molecule binds the siroheme, a buried water molecule (labeled H2O) found in the sulfite-bound SiRHP structure remains at the back of the distal anion-binding pocket in HP_{Em} CrII.

of high phosphate concentrations, photoreduction of SiRHP crystals with proflavin and EDTA in a manner likely to produce a distribution of the three oxidation states with HP −1 dominating (Figure 8B) led to decreased occupancy of phosphate in the active center ($HP-PO_4$ PR2). A more extensively photoreduced crystal (Figure 8C) contained SiRHP with full phosphate occupancy ($HP-PO_4$ PR1) and a structure that is very similar to that of $HP-PO_4$ CrII, which is exclusively composed of HP −2. Thus, the affinity of the one-electron reduced enzyme (HP −1) appears to be less than that of the two-electron reduced enzyme (HP −2) because of phosphate loss in the intermediately reduced crystal ($HP-PO_4$ PR2). Moreover, the solution studies indicate that the affinity of HP −2 for phosphate is considerably less than that of oxidized enzyme (HP).

Dissociation of phosphate from the ferroheme iron is consistent with the intermediate spin state proposed for HP −1 from Mössbuaer, Raman, and NMR spectroscopies (Christner *et al.*, 1983; Han *et al.*, 1989b; Kaufman *et al.*, 1993). Assuming that the valence electrons of siroheme iron retain their d atomic character, an intermediate spin state for the siroheme implies that two electrons reside in the d_{z^2} orbital, which is σ-antibonding to axial ligands (Scheidt & Reed, 1981). Thus, this electronic configuration may reduce the affinity of the siroheme for binding phosphate through oxygen or otherwise increase the exchange rate between phosphate and other ligands. The smaller bond length between Cys483 S^{γ} and the siroheme iron in the intermediately photoreduced structure ($HP-PO_4$ PR2) compared to the oxidized structure ($HP-PO_4$) is consistent with the siroheme iron moving into the ring plane in the reduced states, as monitored by resonance Raman spectroscopy (Han *et al.*, 1989b). The increased structural coupling between the cofactors in HP −1 may be the reason that paramagnetically shifted NMR resonances of Cβ protons on the cysteines ligating the cluster are constant despite the decrease in siroheme spin density from $S = {}^5/_2$ to $S = 1$ (Kaufman *et al.*, 1993).

In solution, binding assays established a K_D of 14 μM for phosphate binding in the active site of the oxidized enzyme. Thus, phosphate likely is the weak-field ligand occupying the sixth coordination position of the siroheme identified by comparing resonance Raman spectra for SiRHP in solution with spectra for a series of model compounds (Melamed *et al.*, 1991). Consistent with the crystallographic structures, phosphate is also released from the active center in solution when the enzyme is reduced (Figure 6). Although our solution experiments do not address which reduced state of the enzyme releases phosphate, the crystallographic structures presented here suggest that the affinity for phosphate is less in HP −1 than in HP −2. The diminished affinity of reduced SiRHP for phosphate in solution and the increased disorder of the active center and surrounding loops for structures with decreased phosphate occupancy (HP_{Em} CrII and $HP-PO_4$ PR2) help explain the difficulty in growing crystals from reduced protein.

In vivo, oxidized SiRHP will certainly bind phosphate because 14 μM is almost 3 orders of magnitude below the 5−8 mM inorganic phosphate concentration found within *E. coli* growing over a pH range of 6.25−8.25 (Kashket, 1982). Expression of the SiR holoenzyme is controlled by the positive transciption activator CysB, which is induced by the cysteine precursor *O*-acetylserine (Kredich, 1987,

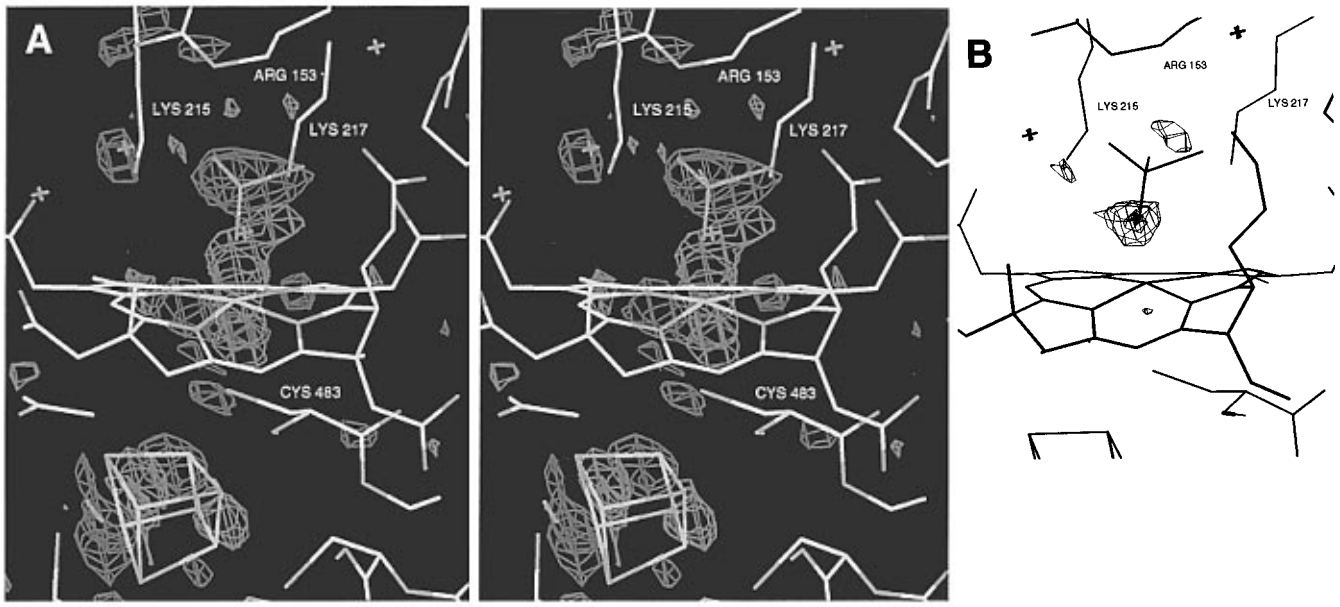

FIGURE 10: Photoreduction to an intermediate reduction state releases phosphate from the SiRHP active center even in the presence of 65 mM Phosphate. (A) Stereoview of the 1.8 Å resolution difference Fourier ($F_{CrII} - F_{PR2}$) electron density map (positive blue contours at 4σ, negative red contours at 4σ) between a crystal assumed completely reduced by Cr(II)EDTA (HP-PO_4 CrII) and a crystal intermediately reduced by photoreduction (HP-PO_4 PR2) indicates that the phosphate ligand and associated, exposed water molecule are at lower occupancy in the intermediately photoreduced crystal. The model refined against the HP-PO_4 PR2 diffraction data (yellow) contains both a partially occupied phosphate and a partially occupied water molecule in the distal coordination site. Large difference peaks around the Fe_4S_4 cluster reflect a slight difference in the position and/or size of the Fe_4S_4 cluster in the two crystals. Increased disorder of the positively charged side chains in HP−PO_4 PR2 compared to HP−PO_4 CrII is indicated by the positive electron density adjacent to Arg153. (B) Residual electron density remaining in the distal anion binding site of the intermediately photoreduced HP-PO_4 PR2 crystal when the phosphate occupancy was set to 0.5. A 1.8 Å resolution difference Fourier ($F_o - F_c$) electron-density map calculated after the SiRHP model was rebuilt and refined against the HP-PO_4 PR2 diffraction data shows a positive density peak ~2.0 Å above the siroheme iron that has been interpreted as a partially occupied water molecule (positive contours are shown at 3σ and 4σ).

1992). Because sulfide is overproduced in a mutant constitutive in the expression of the cysteine regulon (Borum & Monty, 1976), there appears to be little kinetic control of sulfite reduction. However, unlike the upstream sulfur-assimilating enzymes ATP sulfurylase and adenosine 5′-phosphosulfate (APS) kinase, which are rapidly turned over and therefore directly dependent on cysB levels, SiR is quite stable in the cell, resulting in activity that is relatively constant and insensitive to growth phase (Kredich 1971, 1987). Thus, the physiological consequences of the reduction-gated release of an inhibitory phosphate from SiR depend on the reduction state of resting SiRHP inside the cell, which will in turn be related to the availability of NADPH. The intracellular concentrations of NADPH and $NADP^+$ are approximately equal at 100 μM (Neuhard & Nygaard 1987) and both are saturating with respect to SiR. Interestingly, the K_I of SiR for $NADP^+$ is equal to the K_M of SiR for NADPH at 4.5 μM (Siegel *et al.*, 1974). Because the ratio of NADPH/$NADP^+$ remains relatively constant and equal under a variety of growth conditions (Andersen & von Meyenburg, 1977), a large proportion of SiRHP is likely to be oxidized and complexed with phosphate *in vivo*. The role of phosphate may be to stabilize and protect the active site of SiRHP when the enzyme is oxidized and at rest. SiRHP has been optimized to coordinate anions in an active site that, in the absence of an exogenous ligand, is considerably disordered and perhaps susceptible to proteolytic or other degradation. Alternatively, phosphate may prevent other ligands, such as superoxide or peroxide from reacting with the ferric siroheme and producing side products that are detrimental to the cell or lead to deactivation of the enzyme. Oxidized SiRHP has been demonstrated to catalyze dismutation reactions with hydroxylamine[10] that could potentially produce reactive nitrogen oxide species.

In addition to the assimilatory sulfite reductases such as SiRHP, the two other classes of SiRs, the low molecular weight assimilatory enzymes and the dissimilatory enzymes of sulfate-respiring bacteria, may also be activated by reduction through exchange of a heme ligand (Crane & Getzoff, 1996). The low molecular weight SiRs are believed to release an endogenous distal histidine on reduction (Cowan & Sola 1990; Melamed *et al.*, 1991; Lui & Cowan, 1994a), while a dissimilatory sulfite reductase displays a rate-limiting process independent of substrate concentration following reduction of its cofactors (Lui & Cowan, 1994b). Thus, reduction-gated ligand exchange may be a common mechanism among SiRs to stabilize or sequester their active sites in the absence of substrate and reductant. Alternatively, phosphate binding could also simply be an unavoidable consequence of evolving an active site with a large number of positive charges for the recognition and catalytic reduction of sulfite. Phosphate and sulfite also compete with each other for other enzymes within the *E. coli* cell. For example, the F_1F_0 ATP synthase, an enzyme specific for inorganic phosphate, can be competitively inhibited by sulfite (Bakels *et al.*, 1996). Regulatory consequences of competition between metabolically key inorganic anions such as phosphate and sulfite may warrant further attention.

Heme groups have many important roles in enzymatic activity because they allow coupling among electronic states,

[10] L. J. Young and L. M. Siegel, unpublished data.

coordination states, and protein structural states. Often, enzymatic activity is derived from a reciprocal mediation of reactivity between protein components and heme cofactors. The binding and release of endogenous protein side chains or exogenous ligands to the heme iron can serve regulatory roles, controlling reactivity of the metalloporphyrin (Dawson 1988; Raag & Poulos, 1989; Smulevich *et al.*, 1991; Fülop *et al.*, 1995). Proteins exploit balance between electronic, coordination and structural states of the heme iron as a chemical sensor to propagate environmental change to protein conformational change (Perutz, 1979; Yu *et al.*, 1994). Certainly, siroheme plays a central role in the catalytic activity of sulfite reductases and the reactivity of this cofactor is influenced by association with protein. In the context of SiRHP, siroheme is considerably distorted, shares a thiolate ligand with an Fe_4S_4 cluster that is packed against its proximal face, and is involved in an extensive hydrogen-bond network with an array of positively charged residues above its distal face. In a similar vein, the properties of the Fe_4S_4 cluster are influenced by its solvent accessibilty, its interactions with the siroheme, and hydrogen bonds supplied by the protein. The electronic states of the cofactors, so tuned by the protein, are able to directly regulate association with substrate by altering the affinity of the enzyme for an inhibitory phosphate ligand. Reduction of the SiRHP cofactors directly couples changes in the siroheme iron coordination geometry to the increased dynamics and flexibility of active loops, as seen in HP_{Em} CrII, via release of phosphate. In a synergistic fashion, protein and cofactors function together in SiRHP to generate a reduction-gated activation mechanism based on exogenous ligand exchange.

ACKNOWLEDGMENT

We thank D. B. Goodin for assistance with EPR spectroscopy; S. L. Bernstein for her assistance with and efforts in improving the purification of overexpressed SiRHP; J. Wu and N. M. Kredich for providing the *E. coli* sulfite reductase expression system; J. A. Tainer, D. B. Goodin, and N. M. Kredich for valuable discussions and advice; and the Stanford Synchrotron Radiation Laboratory for the use of data collection facilities.

REFERENCES

Andersen, K. B., & von Meyenburg, K. (1977) *J. Biol. Chem. 252*, 4151−4156.

Backes, G., Mino, Y., Loehr, T. M., Meyer, T. E., Cusanovich, M. A., Sweeny, W. V., Adman, E. T., & Sanders-Loehr, J. (1991) *J. Am. Chem. Soc. 113*, 2055−2064.

Bakels, R. H. A., Wielink, J. E. V., Krab, K., & Walraven, H. S. V. (1996) *Arch. Biochem. Biophys. 332*, 170−174.

Bernstein, F. C., Koetzle, T. F., Williams, G. J. B., Meyer, E. F., Jr., Rodgers, J. R., Kennard, O., Shimanouchi, T., & Tasumi, M. (1977) *J. Mol. Biol. 112*, 535−542.

Borum, P. R., & Monty, K. J. (1976) *J. Bacteriol. 125*, 94−101.

Brünger, A. T., Kuriyan, J., & Karplus, M. (1987) *Science 235*, 458−460.

Chakrabarti, P. (1989) *Biochemistry 28*, 6081−6085.

Chang, C. K., & Fajer, J. (1980) *J. Am. Chem. Soc. 102*, 848−851.

Chang, C. K., Hanson, L. K., Richardson, P. F., Young, R., & Fajer, J. (1981) *Proc. Natl. Acad. Sci. U.S.A. 78*, 2652−2656.

Christner, J. A., Münck, E., Janick, P. A., & Siegel, L. M. (1983) *J. Biol. Chem. 258*, 11147−11156.

Cline, J. F., Janick, P. A., Siegel, L. M., & Hoffman, B. M. (1985) *Biochemistry 24*, 7942−7947.

Cline, J. F., Janick, P. A., Siegel, L. M., & Hoffman, B. M. (1986) *Biochemistry 25*, 4647−4654.

Collman, J. P., Sorrell, T. N., Hodgson, K. O., Kulshrestha, A. K., & Strouse, C. E. (1977) *J. Am. Chem. Soc. 99*, 5180−5181.

Connolly, M. L. (1983) *Science 221*, 709−713.

Cowan, J., & Sola, M. (1990) *Inorg. Chem. 29*, 2176−2179.

Crane, B. R., & Getzoff, E. D. (1996) *Curr. Opin. Struct. Biol. 6*, 744−756.

Crane, B. R., & Getzoff, E. D. (1997) *Acta Crystallogr. D53*, 23−40.

Crane, B. R., Siegel, L. M., & Getzoff, E. D. (1995) *Science 270*, 59−67.

Crane, B. R., Belamy, H., & Getzoff, E. D. (1997a) *Acta Crystallogr. D53*, 8−22.

Crane, B. R., Siegel, L. M., & Getzoff, E. D. (1997b) *Biochemistry 36*, 12120−12137.

Czernuszewicz, R. S., Macor, K. A., Johnson, M. K., Gewirth, A., & Spiro, T. G. (1987) *J. Am. Chem. Soc. 109*, 7178−7187.

Dawson, J. H. (1988) *Science 240*, 1308−1319.

Fujita, E., & Fajer, J. (1983) *J. Am. Chem. Soc. 105*, 6743−6745.

Fujita, E., Chang, C. K., & Fajer, J. (1985) *J. Am. Chem. Soc. 107*, 7665−7669.

Fülöp, V., Moir, J. W. B., Ferguson, S. J., & Hajdu, J. (1995) *Cell 81*, 369−377.

Han, S., Czernuszewicz, R. S., Kimura, T., Adams, M. W., & Spiro, T. G. (1989a) *J. Am. Chem. Soc. 111*, 3505−3511.

Han, S., Madden, J. F., Thompson, R. G., Strauss, S. H., Siegel, L. M., & Spiro, T. G. (1989b) *Biochemistry 28*, 5461−5471.

Hendrickson, W. A., Horton, J. R., & LeMaster, D. M. (1990) *EMBO J. 9*, 1665−1672.

Hodel, A., Kim, S. H., & Brünger, A. T. (1992) *Acta Crystallogr. A48*, 851−858.

Janick, P., & Siegel, L. M. (1982) *Biochemistry 21*, 3538−3547.

Janick, P. A., Rueger, D. C., Krueger, R. J., Barber, M. J., & Siegel, L. M. (1983) *Biochemistry 22*, 396−408.

Kashket, E. R. (1982) *Biochemistry 21*, 5534−5538.

Kaufman, J., Spicer, L. D., & Siegel, L. M. (1993) *Biochemistry 32*, 2853−2867.

Kratky, C., Waditschatka, R., Angst, C., Johansen, J. E., Plaquevent, J. C., Schreiber, J., & Eschenmoser, A. (1985) *Helv. Chim. Acta 68*, 1312−1337.

Kredich, N. M. (1971) *J. Biol. Chem. 246*, 3474−3484.

Kredich, N. M. (1987) in *Escherichia coli and Salmonella typhimurium. Cellular and Molecular Biology*. (Neidhardt, F. C., Ed.) Vol. 1, pp 419−428, American Society for Microbiology, Washington, DC.

Kredich, N. M. (1992) *Mol. Microbiol. 6*, 2747−2753.

Krueger, R. J., & Siegel, L. M. (1982) *Biochemistry 21*, 2892−2904.

Kuo, C. F., McRee, D. E., Fisher, C. L., O'Handley, S., Cunningham, R. P., & Tainer, J. A. (1992) *Science 258*, 434−440.

Kuwana (1977) in *Electrochemical Studies of Biological Systems* (Sawyer, D. T., Ed.) ACS Symposium Series, Vol. 38, American Chemical Society, Washington, DC.

Leslie, A. G. W., Brick, P., & Wonacott, A. J. (1986) *CCP4 Newsl. 18*, 33−39.

Lui, S. M., & Cowan, J. A. (1994a) *J. Am. Chem. Soc. 116*, 11538−11549.

Lui, S. M., & Cowan, J. A. (1994b) *Biochemistry 33*, 11209−11216.

Madden, J. F. (1990) Ph.D. Thesis, Department of Biochemistry, Duke University, Durham, NC.

Madden, J. F., Han, S., Siegel, L. M., & Spiro, T. G. (1989) *Biochemistry 28*, 5471−5477.

McRee, D. E. (1992) *J. Mol. Graphics 10*, 44−46.

McRee, D. E., Richardson, D. C., Richardson, J. S., & Siegel, L. M. (1986) *J. Biol. Chem. 261*, 10277−10281.

Melamed, D., Sullivan, E. P., Prendergast, K., Strauss, S. H., & Spiro, T. G. (1991) *Inorg. Chem. 30*, 1308−1319.

Neuhard, J., & Nygaard, P. (1987) in *Escherichia coli and Salmonella typhimurium. Cellular and Molecular Biology* (Neidhardt, F. C., Ed.) Vol. 1, pp 445−473, American Society for Microbiology, Washington, DC.

Noodleman, L., & Case, D. A. (1992) *Adv. Inorg. Chem. 38*, 423−469.
Otwinowski, Z. (1993) in *Data Collection and Processing* (Sawyer, L., Isaacs, N., & Bailey, S., Eds.) pp 56−62, Science and Engineering Research Council, Warrington, UK.
Peck, Jr., H. D., & Lissolo, T. (1988) in *Forty-Second Symposium of the Society for General Microbiology—The Nitrogen and Sulphur Cycles* (Cole, J. A., & Ferguson, S. J., Eds.) Vol. 42, pp 99−132, Cambridge University Press, Cambridge, England.
Perutz, M. F. (1979) *Annu. Rev. Biochem. 48*, 327−386.
Raag, R., & Poulos, T. L. (1989) *Biochemistry 28*, 917−922.
Read, R. J. (1988) *Acta Crystallogr. A42*, 140−149.
Reynolds, M. S., & Holm, R. H. (1989) *Inorg. Chim. Acta 155*, 113−123.
Richardson, J. S., & Richardson, D. C. (1989) in *Prediction of Protein Structure and the Principles of Protein Conformation* (Fasman, G. D., Ed.) pp 217−286, Plenum Press, New York.
Schauer, C. K., Akabori, K., Elliott, C. M., & Anderson, O. P. (1984) *J. Am. Chem. Soc. 106*, 1127−1128.
Scheidt, W. R., & Reed, C. A. (1981) *Chem. Rev. 81*, 543−555.
Siegel, L. M., & Davis, P. S. (1974) *J. Biol. Chem. 249*, 1587−1598.
Siegel, L. M., Murphy, M. J., & Kamin, H. (1973) *J. Biol. Chem. 248*, 251−264.
Siegel, L. M., Davis, P. S., & Kamin, H. (1974) *J. Biol. Chem. 249*, 1572−1586.
Siegel, L. M., Rueger, D. C., Barber, M. J., Krueger, R. J., Orme-Johnson, N. R., & Orme-Johnson, W. H. (1982) *J. Biol. Chem. 257*, 6343−6350.
Smulevich, G., Miller, M. A., Kraut, J., & Spiro, T. G. (1991) *Biochemistry 30*, 9546−9558.
Stephens, P. J., Jollie, D. R., & Warshel, A. (1996) *Chem. Rev. 96*, 2491−2513.
Suh, M. P., Swepston, P. N., & Ibers, J. A. (1984) *J. Am. Chem. Soc. 106*, 5164−5171.
Tan, J., & Cowan, J. A. (1991) *Biochemistry 30*, 8910−8917.
Thompson, G. A. K., & Sykes, A. G. (1976) *Inorg. Chem. 15*, 638−642.
Wiener, H. L., & Reith, M. E. A. (1992) *Anal. Biochem. 207*, 58−62.
Wu, J., Siegel, L. M., & Kredich, N. M. (1991) *J. Bacteriol. 173*, 325−333.
Young, L. J., & Siegel, L. M. (1988a) *Biochemistry 27*, 5984−5990.
Young, L. J., & Siegel, L. M. (1988b) *Biochemistry 27*, 4991−4999.
Yu, A. E., Hu, S., Spiro, T. G., & Burstyn, J. N. (1994) *J. Am. Chem. Soc. 116*, 4117−4118.

BI971065Q